Eur. Phys. J. A manuscript No.
(will be inserted by the editor)

Probing *ab initio* emergence of nuclear rotation

Mark A. Caprio[1], Patrick J. Fasano[1], Pieter Maris[2], Anna E. McCoy[3], James P. Vary[2]

[1]Department of Physics, University of Notre Dame, Notre Dame, Indiana 46556-5670, USA
[2]Department of Physics and Astronomy, Iowa State University, Ames, Iowa 50011-3160, USA
[3]TRIUMF, Vancouver, British Columbia V6T 2A3, Canada

Received: date / Accepted: date

Abstract Structural phenomena in nuclei, from shell structure and clustering to superfluidity and collective rotations and vibrations, reflect emergent degrees of freedom. *Ab initio* theory describes nuclei directly from a fully microscopic formulation. We can therefore look to *ab initio* theory as a means of exploring the emergence of effective degrees of freedom in nuclei. For the illustrative case of emergent rotational bands in the Be isotopes, we establish an understanding of the underlying oscillator space and angular momentum (orbital and spin) structure. We consider no-core configuration interaction (NCCI) calculations for ^{7,9,11}Be with the Daejeon16 internucleon interaction. Although shell model or rotational degrees of freedom are not assumed in the *ab initio* theory, the NCCI results are suggestive of the emergence of effective shell model degrees of freedom ($0\hbar\omega$ and $2\hbar\omega$ excitations) and LS-scheme rotational degrees of freedom, consistent with an Elliott-Wilsdon SU(3) description. These results provide some basic insight into the connection between emergent effective collective rotational and shell model degrees of freedom in these light nuclei and the underlying *ab initio* microscopic description.

1 Introduction

Nuclei are quantum many body systems where the structural phenomena and spectroscopic features characteristically reflect emergent degrees of freedom, from shell structure and clustering to superfluidity and collective rotations and vibrations. These degrees of freedom are traditionally the domain of phenomenological models [1–5], yet their description may be placed on a more fundamental footing if viewed in terms of effective theories built on a microscopic description. Indeed, the emergent phenomena of nuclear structure may be viewed as simply the topmost tier in a tower of effective theories of nuclear physics beginning at the subnucleonic level [6, 7].

Ab initio nuclear theory attempts a direct description explicitly from the fully microscopic formulation of the many-body system in terms of nucleons and their free-space interactions. An accurate treatment of correlations can be computationally challenging, but *ab initio* theory now reproduces signatures of emergent phenomena, including clustering [8–12] and rotation [13–16], primarily in light nuclei. We can look therefore to *ab initio* theory as a means of exploring the emergence of effective degrees of freedom from a microscopic foundation, and understanding their place within the full description of nuclear properties and spectroscopy.

To explore the physical structure of emergent rotation in some of the lightest nuclei, and to gain some insight into the nature of the relevant effective degrees of freedom, we consider here a few illustrative "case studies" of rotational bands in *ab initio* no-core configuration interation (NCCI) [17], or no-core shell model (NCSM), calculations of the odd-mass Be isotopes, specificially, ^{7,9,11}Be.

Some of these rotational bands (or portions thereof) have been studied before in NCCI calculations [13–16, 18]. However, these earlier calculations, which were based on internucleon interactions such as JISP16 [19] and $\mathrm{NNLO}_{\mathrm{opt}}$ [20], suffered from a significant limitation: excited rotational bands were relatively poorly converged in the many-body calculations, lying at much higher excitation energy than they would either in a more completely converged calculation for those interactions or, indeed, in experiment. In practice, this meant that portions of the bands, especially at lower angular momentum, lay in regions of the spectrum

where the calculated level density was high, and mixing or fragmentation consequently tended to obscure these bands.

Here we make use of the much softer Daejeon16 internucleon interaction [21], which permits more rapidly convergent NCCI calculations. This interaction is obtained starting from the classic Entem-Machleidt N^3LO chiral perturbation theory interaction [22], which is then softened via a similarity renormalization group transformation and subsequently adjusted via a phase-shift equivalent transformation to yield an accurate description of light nuclei with $A \leq 16$.

In cases where only fragmented precursors of excited rotational bands were obtained in previous calculations, these bands are now found low in the excitation spectrum, and approaching their converged energies. Improved convergence means not only that the rotational energies themselves are more accurately described, but that the band structure itself becomes clearer. The cleaner rotational spectrum, comparatively free from fragmentation, permits easier interpretation and understanding of the electric quadrupole ($E2$) transition spectroscopy.

Improved convergence also, in principle, allows more meaningful identification of experimentally observed counterparts to the rotational states. However, doing so requires detailed understanding of the energy convergence and, for the less completely converged energies, likely still entails some form of basis extrapolation [23–28]. Our focus here will thus primarily be restricted to the nature of the emergent structure arising in solving the many-body problem, rather than detailed comparison with experiment (*e.g.*, Refs. [29, 30]).

Beyond simply analyzing the spectroscopic signatures of emergent phenomena appearing in *ab initio* calculations, we can make use of microscopic wave functions obtained in these calculations to directly probe for structural insight. In the following discussions, we examine the decompositions of the wave functions in terms of oscillator excitations (*i.e.*, "$0\hbar\omega$" and "$2\hbar\omega$ or higher contributions) and spin and orbital angular momentum contributions. We build here on Johnson's analysis [18] of the angular momentum structure of rotational states.

In characterizing effective theories of emergent nuclear phenomena, we consider not only emergent degrees of freedom, but also emergent symmetries. Dynamical symmetries [31–34] in general can be responsible for the emergence of simple patterns in the behavior of complex systems. In the traditional shell model, Elliott's SU(3) dynamical symmetry [35–38] provides a mechanism for the emergence of rotation, as arising naturally within the SU(3) irreducible representations (irreps) preferred by a quadrupole-quadrupole interaction. The symplectic group $\mathrm{Sp}(3,\mathbb{R})$, which contains Elliot's SU(3) as a subgroup, and the multishell symplectic shell model associated with this group, has then been proposed as providing a microscopic formulation of the unified collective model [39–41]. Wave functions obtained in *ab initio* calculations have indeed been found to receive strong contributions from specific dominant U(3) or $\mathrm{Sp}(3,\mathbb{R})$ symmetry components [42–46]. We shall therefore comment, at least briefly, on how the rotational structures considered here can relate to such symmetries.

In the following explorations, we begin with ^{9}Be (Sec. 3). The low-lying rotational bands in both the natural (negative) parity and unnatural (positive) parity spaces provide particularly clean illustrations of the angular momentum structure of the rotational bands and the implications of Elliott SU(3) dynamical symmetry.

Then ^{11}Be (Sec. 4) provides an example of the coexistence of $0hw$ and $2\hbar\omega$ rotational bands within the same spectrum, and thus of rotation outside the effective space of the $0\hbar\omega$ shell model.

Finally, ^{7}Be (Sec. 5) introduces the qualitatively distinct situation in which the $0\hbar\omega$ ground state band is connected by strong $E2$ transitions to a $2\hbar\omega$ excited band. This excitation may be understood in terms of $\mathrm{Sp}(3,\mathbb{R}) \supset \mathrm{U}(3)$ dynamical symmetry [47, 48]. In the macroscopic limit, it would be construed as representing the excitation of an effective giant quadrupole degree of freedom.

However, we first (Sec. 2) lay out the excitation spectra obtained in *ab initio* NCCI calculations for all three nuclei. In preparation for the following discussions, we review the basic spectroscopic properties of nuclear rotations, as well as stress the importance of considering convergence (with respect to the basis for the NCCI calculation) in interpreting any such results.

2 Rotational signatures and overview of calculations

2.1 Rotational spectra

Rotational bands are commonly recognized (whether in experiment or in calculations) by energies following the rotational formula, relative $E2$ strengths following the rotational formulas (Alaga rules) [49], and enhanced $E2$ strengths overall. In terms of the physical structure of the rotational band members, these features arise from a shared intrinsic structure, combined with a different overall rotational motion, for the different members of the same rotational band. That is, in ideal rotation,

there is an adiabatic separation of degrees of freedom, between a rotational intrinsic state and the collective rotational coordinates (Euler angles). In the case of an axially symmetric intrinsic state $|\phi_K\rangle$, the angular momentum is characterized by a definite projection K onto the intrinsic symmetry axis, and the rotational band members have angular momenta $J \geq K$, with wave functions [50]

$$|\psi_{JKM}\rangle \propto \int d\vartheta \left[\mathscr{D}^J_{MK}(\vartheta) \, |\phi_K;\vartheta\rangle + (-)^{J+K} \mathscr{D}^J_{M,-K}(\vartheta) \, |\phi_{\bar{K}};\vartheta\rangle \right], \quad (1)$$

where the Wigner $\mathscr{D}$ function constitutes the wave function in the collective rotational Euler angle coordinate ϑ, while $|\phi_K;\vartheta\rangle$ represents the intrinsic state after rotation by Euler angles ϑ. The second term, involving the conjugated intrinsic state $|\phi_{\bar{K}}\rangle$ with angular momentum projection $-K$ along the intrinsic symmetry axis, arises to preserve symmetry under rotation by an angle π about an axis perpendicular to the symmetry axis.

Band members are then expected to have energies following the rotational formula

$$E(J) = E_0 + AJ(J+1), \quad (2)$$

where the rotational energy constant $A \equiv \hbar^2/(2\mathcal{J})$ is inversely related to the moment of inertia $\mathcal{J}$ of the rotational intrinsic state, and the intercept parameter $E_0 = E_K - AK^2$ is related to the energy E_K of the rotational intrinsic state. However, for $K = 1/2$ bands, the Coriolis contribution to the kinetic energy significantly modifies the energies, leading to an energy staggering which is given, in first-order perturbation theory, by

$$E(J) = E_0 + A\big[J(J+1) + a(-)^{J+1/2}(J+\tfrac{1}{2})\big], \quad (3)$$

where the Coriolis decoupling parameter a depends upon the structure of the rotational intrinsic state.

The excitation spectra obtained in NCCI calculations for the odd-mass isotopes ^{7,9,11}Be are shown in Figs. 1–3, with energies against an angular momentum axis scaled as $J(J+1)$, as appropriate for rotational energy analysis. The states identified with the rotational bands discussed in the following are highlighted (red outlines). The $E2$ transitions from these levels are shown, specifically, for angular-momentum decreasing transitions originating from band members. The line thicknesses (and shadings) indicate transition strengths. Further details of the calculations are defined below.

For the bands in Figs. 1–3, the energies expected from the rotational energy relations (2) or (3) are shown as best fit lines. [For the $K = 1/2$ bands, the three parameters in (3) are simply determined to match the calculated energies of the three lowest-energy band members.]

A common criterion for identifying rotational band members is that, loosely speaking, $E2$ strengths between rotational band members are expected to be "enhanced". The $E2$ matrix elements within a rotational band follow the Alaga relations, and thus all $E2$ matrix elements within a band should follow a pattern of *relative* intensities given by Clebsch-Gordan coefficients. Then, the overall *scale* of the intensities is determined by the $E2$ matrix element within the intrinsic state or, equivalently, by the intrinsic quadrupole moment Q_0. (Similar relations apply to interband transitions between the same two rotational bands, with the overall strength given by an interband intrinsic matrix element.) For $B(E2)$ strengths (*i.e.*, reduced transition probabilities) within a band, the rotational relation becomes

$$B(E2; J_i \to J_f) = \frac{5}{16\pi}(J_i K 20|J_f K)^2 (eQ_0)^2. \quad (4)$$

This relation yields the strengths in Fig. 4, where different curves apply depending upon K for the band, which, for an ideal $K = 1/2$ band, gives the transition pattern illustrated in Fig. 5.

Consequently, $E2$ transitions within a band are enhanced to the extent that the intrinsic matrix element is larger than the typical scale of $E2$ matrix elements between arbitrary states not within a band. This is commonly the case, as rotation is associated with quadrupole deformation. Even so, it is worth keeping in mind that not all transitions within a rotational band are expected to be "strong", if they are suppressed by the Clebsch-Gordan coefficient, *e.g.*, for the $K = 1/2$ band (Fig. 5), the $\Delta J = 1$ transitions (with the exception of the $3/2 \to 1/2$ band head transition) are highly suppressed relative to the $\Delta J = 2$ transitions.

2.2 Convergence of rotational observables

The NCCI approach is based upon expressing the nuclear many-body system in terms of a basis of antisymmetrized products (Slater determinants) of harmonic oscillator single-particle states. The many-body Hamiltonian is represented as a matrix in terms of this basis, and the energy eigenvalues and wave functions are obtained by solving the (large) matrix eigenproblem which ensues.

Calculations must, of course, be carried out in a finite, truncated basis, and the results depend upon this truncation. Each basis state represents a configuration

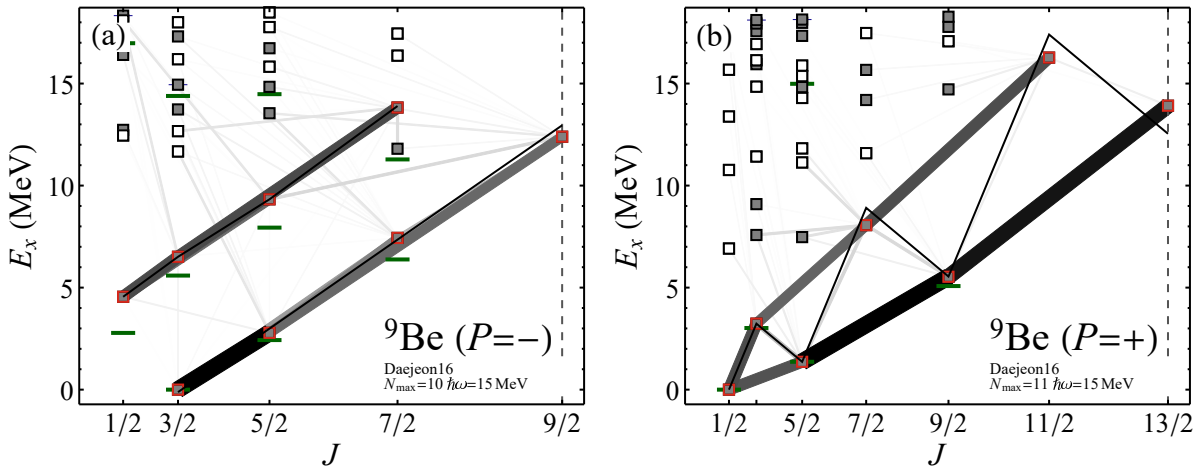

Fig. 1 *Ab initio* calculated energy spectra for ^{9}Be (a) negative and (b) positive parity, obtained for the Daejeon16 interaction. Calculations are with basis truncations $N_{\max} = 10$ and 11, respectively, and oscillator basis parameter $\hbar\omega = 15\,\mathrm{MeV}$. Experimental energies (green horizontal lines) are shown for comparison (see text). Rotational band members are highlighted (red squares), and rotational energy fits are indicated by lines. The J-decreasing $E2$ transitions originating from these rotational band members are shown (specifically, transitions with $J_f < J_i$ or with $J_f = J_i$ and $E_f < E_i$), where the line thickness (and shading) is directly proportional to the $B(E2)$ strength. States are approximately classified as $0\hbar\omega$ (filled symbols) or $2\hbar\omega$ (open symbols) for natural parity, or similarly $1\hbar\omega$ and $3\hbar\omega$ for unnatural parity, classified by the dominant oscillator configuration (see Sec. 3.2), and states with isospin $T > |T_z|$ are indicated by tick marks. The maximal valence angular momentum, *i.e.*, the largest which can be constructed in the $0\hbar\omega$ or $1\hbar\omega$ space, respectively, is indicated by the vertical dashed line. Excitation energies are taken separately within each parity.

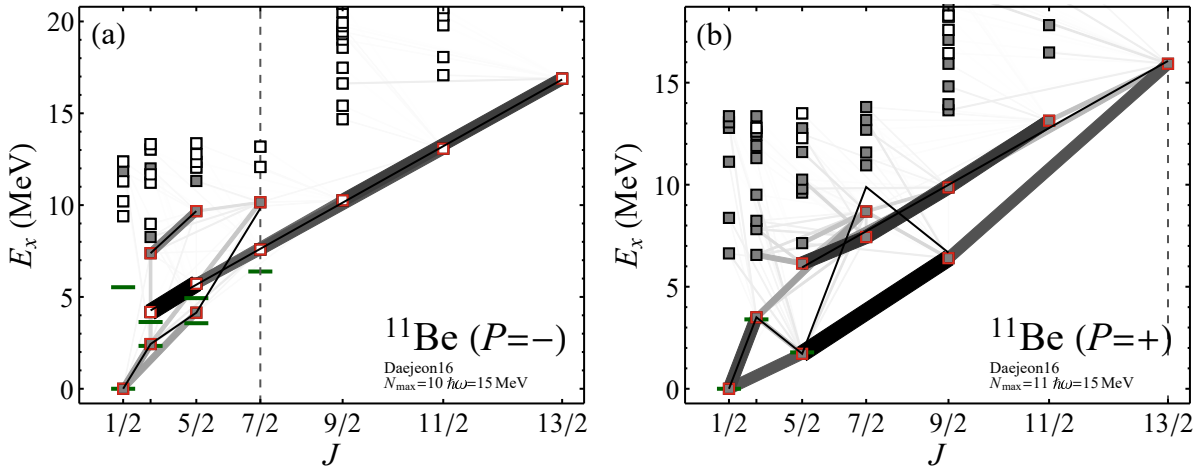

Fig. 2 *Ab initio* calculated energy spectra for ^{11}Be (a) negative and (b) positive parity, obtained for the Daejeon16 interaction, with basis truncations $N_{\max} = 10$ and 11, respectively. See Fig. 1 caption for further description of figure contents and labeling.

of nucleons distributed over oscillator shells, and is thus characterized by the number N_{ex} of oscillator excitations above the lowest Pauli-allowed filling of oscillator shells. The basis is commonly constrained by limiting the number of excitations to $N_{\mathrm{ex}} \leq N_{\max}$. (Results obtained with a truncated basis also depend upon the underlying oscillator length scale [51] defining the basis, given by the basis parameter $\hbar\omega$.) However, as $N_{\max}$ increases, results converge towards those which would be obtained in the full, untruncated many-body space, and thus also must become independent of the basis parameter $\hbar\omega$.

The results shown in Figs. 1–3 are obtained in spaces truncated to $N_{\max} = 10$ or 11 for ^{9,11}Be (Figs. 1–2) and $N_{\max} = 14$ for ^{7}Be.[1] These calculations were obtained

[1] For odd-mass p-shell nuclei, as considered here, note that the "natural" parity, obtained with the lowest allowed filling of harmonic oscillator shells, as in a traditional "$0\hbar\omega$" shell model description, is negative parity. An NCCI basis consisting of configurations with even numbers of oscillator excitations ($N_{\mathrm{ex}} = 0, 2, \ldots$), and thus having an even $N_{\max}$,

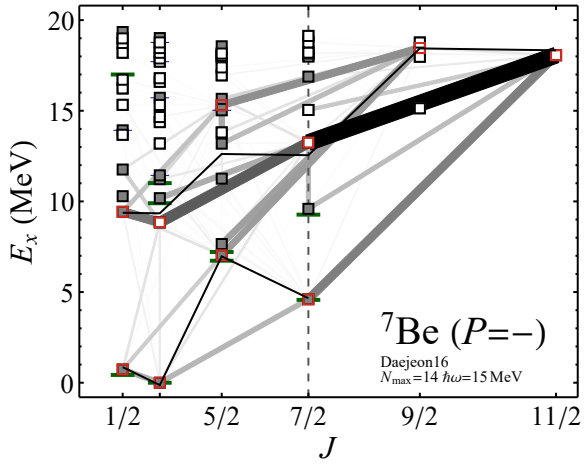

Fig. 3 *Ab initio* calculated energy spectra for ^{7}Be negative parity, obtained for the Daejeon16 interaction, with basis truncation $N_{\max} = 14$. See Fig. 1 caption for further description of figure contents and labeling.

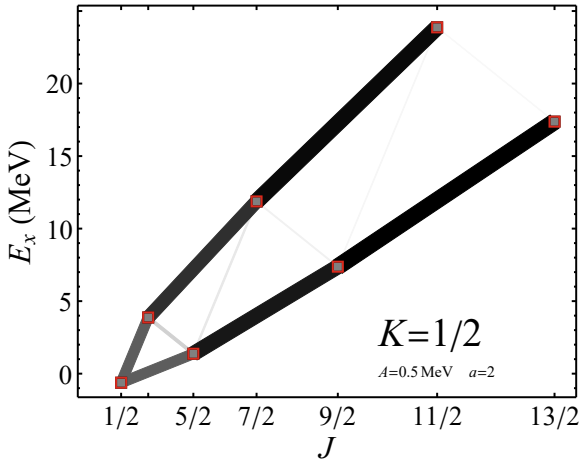

Fig. 5 Rotational predictions for $B(E2)$ strengths within an ideal $K = 1/2$ band. The line thickness (and shading) is directly proportional to the $B(E2)$ strength.

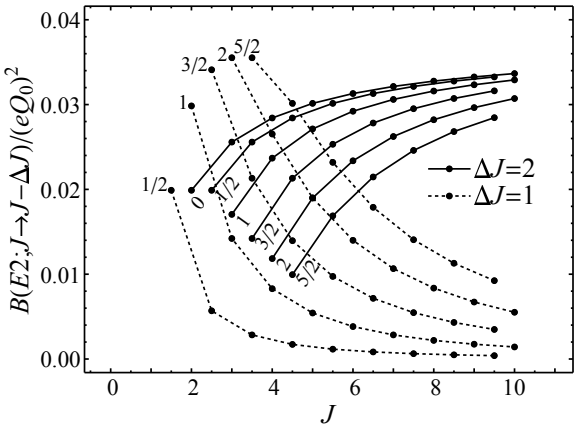

Fig. 4 Rotational Alaga rule predictions for $B(E2)$ strengths within a rotational band, normalized to the square of the intrinsic quadrupole moment Q_0, shown separately for $\Delta J = 2$ (solid curves) and $\Delta J = 1$ (dotted curves) transitions. Curves are shown for bands with $0 \le K \le 5/2$, as indicated.

based on the Daejeon16 interaction plus Coulomb interaction, with oscillator basis parameter $\hbar\omega = 15$ MeV (roughly corresponding to the variational minimum energy), using the M-scheme NCCI code MFDn [52–54]. Initial results from the present calculations were included in Refs. [29, 30].

The accuracy which can be obtained in solving the many-body problem is limited by the highest $N_{\max}$-truncated spaces which are computationally accessible. In ^{9}Be, an $N_{\max} = 13$ space (dimension $\sim 1.1 \times 10^{10}$) pushes the limits of current computational capabilities.

yields the natural parity space, while an NCCI basis consisting of configurations with odd numbers of oscillator excitations ($N_{\rm ex} = 1, 3, \ldots$), and thus odd $N_{\max}$, yields the unnatural parity space.

The dependence of calculated energies on the truncation $N_{\max}$, as well as on the basis parameter $\hbar\omega$, may be seen for the ground state $3/2^-_1$ (solid curves) and ground state rotational band member $5/2^-_1$ (dashed curves) of ^{9}Be in Fig. 6(a). While the curves corresponding to succesive steps in $N_{\max}$ are coming closer together, and flattening in their dependence on $\hbar\omega$ as well, the calculated energy eigenvalues are still changing by amounts on the order of 1 MeV with each step in $N_{\max}$, even near the variational minimum ($\hbar\omega \approx 15$ MeV). The use of softened interactions, such as the Daejeon16 interaction considered here, ameliorates but clearly does not eliminate the challenge of convergence.

Given that the rotational spacings are also on the order of MeV, it is not *a priori* clear that detailed features of the rotational spectrum should be well-resolved in the calculations. Yet, despite limitations in convergence, the rotational pattern of energy spacings is readily apparent. While the energy eigenvalues of the individual states with a band may be decreasing with $N_{\max}$, the energies of states belonging to the same band decrease together.

Returning to the lowest $3/2^-$ and $5/2^-$ states in ^{9}Be, consider their energy difference, giving the excitation energy of the $5/2^-$ state within the band, shown in Fig. 6(b). This difference flattens in $\hbar\omega$ in the vicinity of $\hbar\omega = 15$ MeV, where it is changing by $\lesssim 0.05$ MeV for each step in $N_{\max}$. We will note the degree of convergence of relative energies within specific bands, as well as of the excitation energies of bands relative to each other, as we explore the band structure in more detail in the following sections.

For calculated $E2$ strengths, the convergence challenge is even more dramatic. The dependences of the

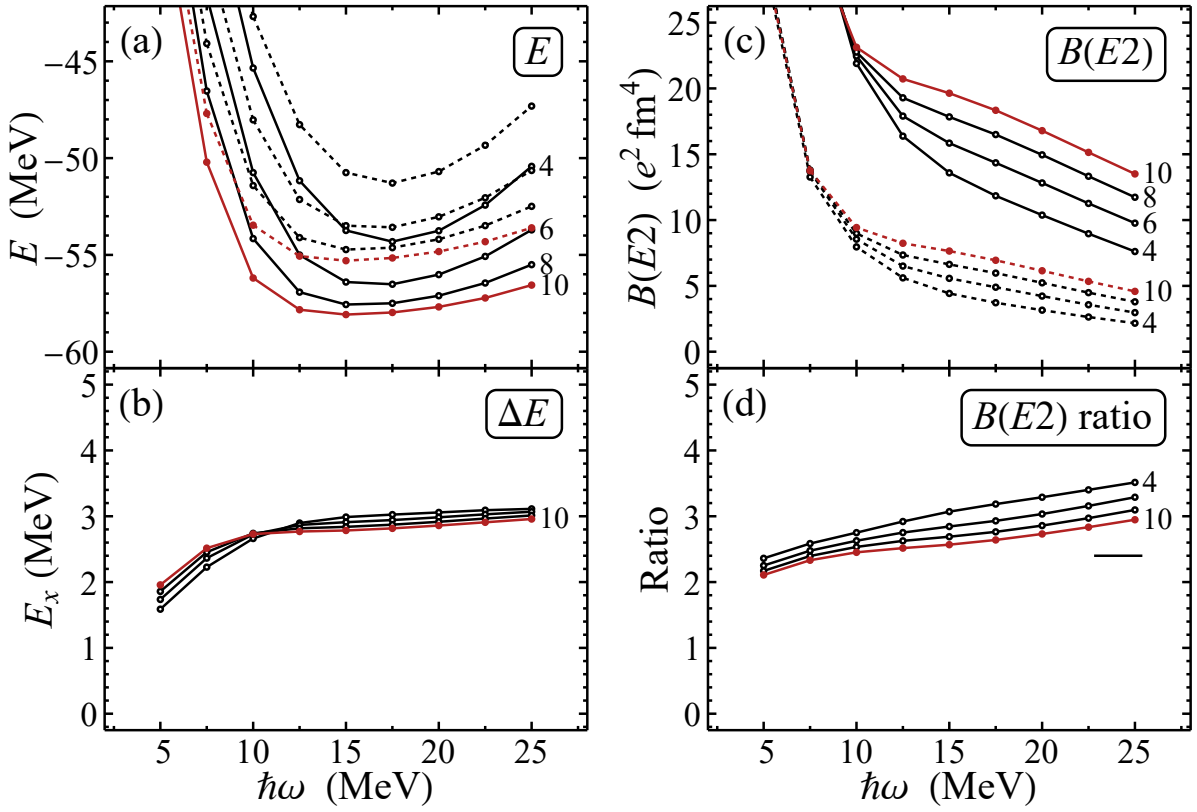

Fig. 6 Convergence of calculated energy and transition observables for ^{9}Be (top) and corresponding relative observables (bottom): (a) Energies of the $3/2^-_1$ ground state (solid curves) and $5/2^-_1$ rotational band member (dashed curves). (b) The energy difference $E(5/2^-) - E(3/2^-)$. (c) Transition strengths $B(E2; 5/2^- \to 3/2^-)$ (solid curves) and $B(E2; 7/2^- \to 3/2^-)$ (dashed curves) within the ground state rotational band. (d) The transition strength ratio $B(E2; 5/2^- \to 3/2^-)/B(E2; 7/2^- \to 3/2^-)$. The Alaga ratio 12/5 is shown for comparison (horizontal bar). Calculated values are shown as functions of the basis parameter $\hbar\omega$, for $N_{\max} = 4$ to 10 (as labeled).

calculated $E2$ strengths, on $N_{\max}$ and $\hbar\omega$, are shown for the $5/2^- \to 3/2^-$ (solid curves) and $7/2^- \to 3/2^-$ transitions within the ground state band in Fig. 6(c). Neither set of curves, for either transition (solid and dashed curves, respectively), is obviously approaching any particular stable, converged value. Yet, the relative transition strengths among members of the same band are already well-established at low $N_{\max}$, with the ratios of transition strengths approximately following Alaga rotational relations (see Figs. 6–8 and 17 of Ref. [14] for quantitative analyses). Returning to the $5/2^- \to 3/2^-$ and $7/2^- \to 3/2^-$ transitions of Fig. 6(c), both families of curves have the same general shape, differing rather in scale. Taking the ratio of calculated values, $B(E2; 5/2 \to 3/2)/B(E2; 7/2 \to 3/2)$, gives the values shown in Fig. 6(d). While these are clearly not strictly converged, there is a clear "shoulder" (inflection) in the $\hbar\omega$ dependence in the vicinity of $\hbar\omega = 15\,\mathrm{MeV}$, where the ratio is changing by $\lesssim 5\%$ for each step in $N_{\max}$. The values may be compared to the Alaga ratio $12/5\,(= 2.4)$, from (4), for an ideal $K = 3/2$ band.

Converged values for observables reflect an accurate solution of the many-body problem as it has been mathematically formulated. Whether or not the ensuing values are in agreement with experiment is an entirely separate question. Success depends not only on solving the many-body problem as it has been stated, but on the fidelity of this many-body problem to the physical system in the first place and, in particular, on the accuracy of the internucleon interaction taken as input to the calculation. That is, success also depends on the structural integrity of the underlying layers in the tower of effective theories.

While we attempt to provide some basic contact with experimental excitation spectra for comparison in Figs. 1–3 (horizontal lines), the spin-parity assignments of many experimentally observed levels are unknown or uncertain, and conflicting spin-parity assignments are found in the literature. For simplicity, the experimental levels shown in Figs. 1–3 are those assigned a unique angular momentum and parity in the current experimental evaluations [55–57], regardless of whether or

not this assignment is designated as tentative, with one exception in ^{11}Be.[2]

3 ^{9}Be: *LS* coupling scheme and Elliott rotation in the valence shell

3.1 Rotational spectrum and convergence

The rotational spectrum of ^{9}Be provides a starting point for illustrating many of the essential features of rotation, building on discussions of the rotational structure of ^{9}Be from prior NCCI calculations [14, 16, 18]. The near-yrast states in the low-lying calculated spectrum of ^{9}Be form three rotational bands: in the negative parity spectrum [Fig. 1(a)], a $K^P = 3/2^-$ ground state (yrast) band and $K^P = 1/2^-$ excited (yrare) band, and then, in the positive parity spectrum [Fig. 1(b)], a $K^P = 1/2^+$ yrast band. These rotational bands may be recognized from the energies, which approximately follow the expected rotational energy spacings (with staggering for the $K = 1/2$ bands), and from the enhanced $E2$ connections between band members.

The main qualitative features of the rotational bands are robustly calculated, that is, with only small residual dependences on the truncation of the calculation. The excitation energies of band members are shown for successive values of $N_{\max}$ in Fig. 7. We may summarize the general features, which are consistent with the earlier calculations with other interactions (see Fig. 16 of Ref. [14]). The excitation energies of the two $K = 1/2$ bands relative to the ground state are not as well converged as the spacings within bands, but much better than the energy eigenvalues themselves. The $K^P = 1/2^-$ excited band would appear to be rapidly converging in excitation energy, towards an energy lower than that found at $N_{\max} = 10$ but within $\sim 1\,$MeV [29]. The staggering of energies within the calculated $K^P = 1/2^-$ band decreases with increasing $N_{\max}$ and is consistent with zero ($a \lesssim 0.1$) [Fig. 7(a)]. The staggering within the $K^P = 1/2^+$ band, in contrast, is pronounced ($a \approx 2$) [Fig. 7(b)].

All three bands in the low-lying spectrum of ^{9}Be terminate, and they do so at angular momenta consistent with a simple $0\hbar\omega$ or $1\hbar\omega$ shell model picture. For negative parity, the maximal angular momentum which can be constructed by coupling of the valence nucleons in the p shell, in a $0\hbar\omega$ description of ^{9}Be, is $9/2$ [indicated by the vertical dashed line in Fig. 1(a)]. The $K^P = 3/2^-$ band terminates at $J = 9/2$, while the $K^P = 1/2^-$ band terminates at the lower angular momentum $J = 7/2$. For positive parity, the maximal angular momentum which can be generated in a $1\hbar\omega$ description of ^{9}Be, in particular, by exciting one valence nucleon from the p shell to the sd shell, is $J = 13/2$ [indicated by the vertical dashed line in Fig. 1(b)]. The $K^P = 1/2^+$ band likewise terminates at this angular momentum.[3]

The patterns of $E2$ transitions within the bands are generally consistent with those expected from the Alaga rotational relations (Fig. 4). For instance, for the $K^P = 1/2^+$ band, for which the transitions are most clearly visible in the figure, due to the separation between lines afforded by the energy staggering [Fig. 1(b)], we may compare to the similar pattern for an ideal $K = 1/2$ band (Fig. 5).

There is also a somewhat enhanced *interband* transition between the negative parity bands [Fig. 1(a)], from the $J = 9/2$ terminating member of the ground state band to the $J = 5/2$ member of the excited band (noted also in Fig. 14 of Ref. [16]). While interband transitions are certainly possible in a rotational picture, these are expected to follow Alaga rotational relations, in which all transition matrix elements between the same two bands are proportional to a common intrinsic interband transition matrix element [50]. This single enhanced $9/2^-_1 \to 5/2^-_2$ transition, without, say, a comparably enhanced $7/2^-_1 \to 3/2^-_2$ transtion, is not expected in a simple axially symmetric rotational picture. Rather, it appears to represent a band termination effect reflecting the limited dimension of the $0\hbar\omega$ shell model space, which admits only one $J = 9/2$ state, to be "shared" between the bands (see also Sec. 3.3 below).

3.2 Structure in oscillator space

A natural first question is then whether or not the rotational structure presented by these states might have an effective description within a simple valence shell model space ($0\hbar\omega$ or $1\hbar\omega$, for negative and positive parity, respectively). The calculated states in Fig. 1(a) can be loosely identified as "$0\hbar\omega$" or "$2\hbar\omega$" (or higher

[2] The experimental level at 3.4 MeV excitation energy in ^{11}Be, which is only identified as $(3/2^-, 3/2^+)$ in Ref. [57], is shown as $3/2^-$ in Fig. 2(a), consistent with the rotational analysis of Refs. [58, 59], where it is taken as a $K^P = 3/2^-$ band head. See discussion in footnote 6 of Ref. [29].

[3] The yrast $15/2^+$ and $19/2^+$ states were considered in Refs. [14, 16] as possible extended members of the $K^P = 1/2^+$ band, on the basis of strong $E2$ transitions to the $11/2^+_1$ and $13/2^+_1$ band members, but these states lie at energies above what would be expected from the rotational energy formula. These states would now seem more likely to be members of a higher-lying excited rotational band with strong interband transitions, as discussed in detail for the illustrative case of ^{7}Be in Sec. 5.

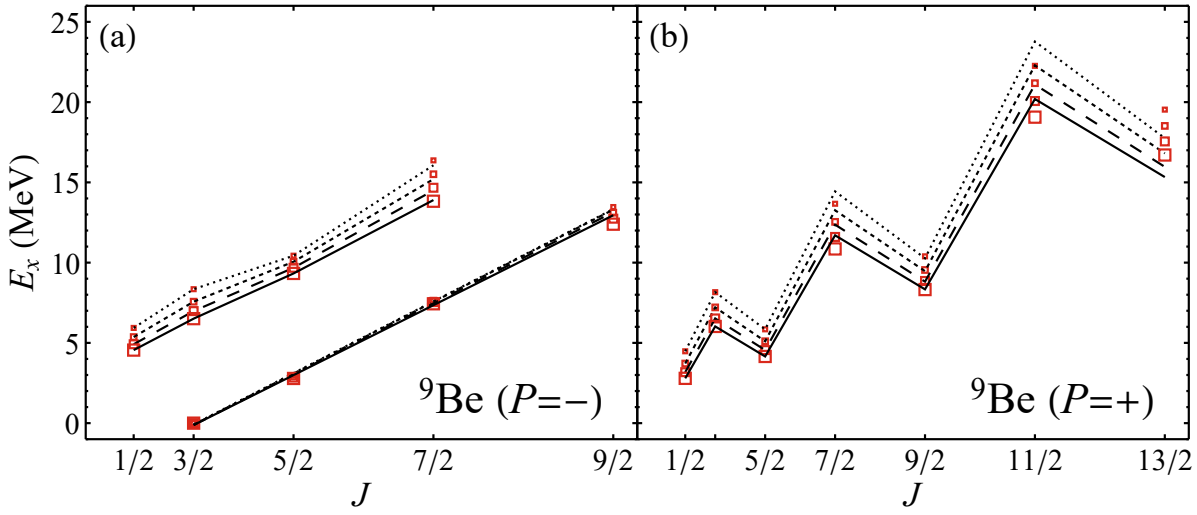

Fig. 7 Calculated energies for rotational band members in ^{9}Be, for (a) negative and (b) positive parity, shown as excitation energies relative to the negative parity ground state. The calculated bands are for $N_{\max} = 4$ to 10 or $N_{\max} = 5$ to 11, respectively (dotted through solid curves).

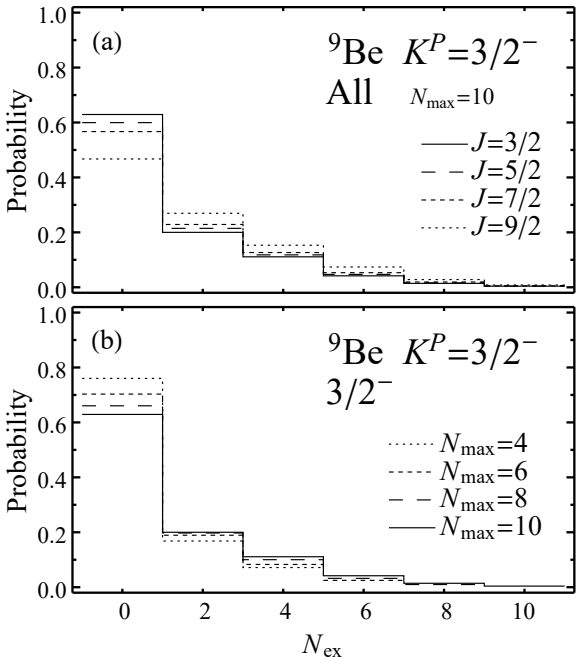

Fig. 8 Decompositions of ^{9}Be $K^P = 3/2^-$ ground state band members, with respect to number of excitation quanta $N_{\rm ex}$ in the contributing oscillator configurations: (a) Decompositions of all band members $3/2 \le J \le 9/2$ (solid through dotted curves), as calculated for $N_{\max} = 10$. (b) Decomposition of the $3/2^-$ band head (*i.e.*, the ground state), as calculated for $N_{\max} = 4$ to 10 (dotted through solid curves).

$N_{\rm ex}\hbar\omega$) states, in traditional shell model terminology, based on their decompositions in the harmonic oscillator basis. Similarly the calculated states in Fig. 1(b) can be loosely identified as "$1\hbar\omega$" or "$3\hbar\omega$" (or higher $N_{\rm ex}\hbar\omega$).

The contributions from configurations of different $N_{\rm ex}$ to the wave function norm (or probability) are shown in Fig. 8, for the calculated wave functions of the ground state band members. The contribution from $N_{\rm ex} = 0$ dominates in each band member [Fig. 8(a)], although the details are dependent upon the truncation of the calculation [Fig. 8(b)]. In general, some of this probability "bleeds off" to higher $N_{\rm ex}$ as the wave functions are calculated in higher $N_{\max}$ spaces. The rough classification of states as $0\hbar\omega$ or $2\hbar\omega$ (shaded and open symbols, respectively) in Figs. 1–3 is determined simply by considering whether the largest contribution to the wave function comes from $N_{\rm ex} = 0$ oscillator many-body basis states or $N_{\rm ex} = 2$ oscillator many-body basis states [30, 60] (the classification into $1\hbar\omega$ and $3\hbar\omega$ states for unnatural parity is accomplished similarly).

Examination of the different oscillator-basis $N_{\rm ex}$ contributions is suggestive, and provides a potentially valuable diagnostic tool to recognize qualitative patterns in the calculated spectra (as in the following Secs. 4 and 5). However, it is important to keep in mind that the $N_{\rm ex}$ decomposition in an oscillator basis is at best an approximate indicator of structure, even aside from the dependence on the $N_{\max}$ truncation of the calculation. We may at most loosely identify $N_{\rm ex}\hbar\omega$ excitations in an oscillator basis with $N_{\rm ex}\hbar\omega$ excitations in the traditional shell model, which are taken to be particle-hole excitations above a physically-meaningful mean-field (*e.g.*, Hartree-Fock) vacuum. Furthermore, even for fully converged calculations of the exact same wave function, different results are obtained for the de-

composition into oscillator basis functions, depending upon the choice of length scale (or $\hbar\omega$ parameter) for the oscillator basis into which the decomposition is being carried out (here, recall, we are working with a basis parameter of $\hbar\omega = 15\,\mathrm{MeV}$, chosen near the variational energy minimum for calculations with the Daejeon16 interaction).

Nonetheless, for the calculated ^{9}Be rotational band members, the dominance of $N_{\rm ex} = 0$ contributions suggests that an effective description in the valence shell may not be unreasonable. Such an effective description could be approached through, *e.g.*, reformulation of the *ab initio* problem in a valence space obtained through application of the in-medium similarity renormalization group (IM-SRG) [61].

3.3 Angular momentum structure

The LS angular momentum coupling scheme is understood to play a significant role in the structure of p-shell nuclei, in possible competition with the jj coupling scheme which becomes predominant in heavier nuclei [62, 63]. While jj coupling refers to the role of single-particle j orbitals, the concept of LS coupling is independent of choice of single-particle basis, or even the concept of a single-particle basis. It is defined rather in term of the total orbital (spatial) angular momentum $\mathbf{L}$ of the nucleons, and their total spin angular momentum $\mathbf{S}$, by the condition that the many-body state have sharp angular momenta L and S, combining to give the total J.[4]

That the *ab initio* calculated negative parity rotational band members of ^{9}Be largely obey LS coupling was demonstrated in Ref. [18], in the context of calculations with the Entem-Machleidt N^{3}LO interaction. The portion of any NCCI calculated wave function coming from contributions with a given L or S is not manifest from its expansion in a tradititional M-scheme basis, but the so-called "Lanczos trick"[5] may be used to decompose the original calculated wave function into contributions from the different eigenspaces of $\mathbf{L}^2$ and $\mathbf{S}^2$, and thus according to L and S.

For the ^{9}Be negative parity band members, the L and S decompositions from the present calcuations with the Daejeon16 interaction are shown in Fig. 9. The salient feature of the LS structure, discussed for the earlier calculations in Refs. [16, 18], is that the dominant L contributions for successive band members are $L = 1$, 2, 3, and 4, while the spin is predominantly $S = 1/2$. In the ground state $K^P = 3/2^-$ band, the angular momenta are coupled in the "aligned" sense, giving $J = L + 1/2$, and thus $J = 3/2$, 5/2, 7/2, 9/2. In the excited $K^P = 1/2^-$ band, these same angular momenta are coupled in the "antialigned" sense, giving $J = L - 1/2$, and thus $J = 1/2$, 3/2, 5/2, 7/2.

A more concise overview of the angular momentum structure of these bands is obtained by considering a single "effective" (or mean) orbital angular momentum $\bar{L}$ for each state, defined in terms of the expectation value of the $\mathbf{L}^2$ operator as[6]

$$\bar{L}(\bar{L}+1) \triangleq \langle \mathbf{L}^2 \rangle. \tag{5}$$

Effective proton spin, neutron spin, and spin angular momenta ($\bar{S}_p$, $\bar{S}_n$, and $\bar{S}$, respectively) may be obtained similarly, *e.g.*, $\bar{S}(\bar{S}+1) \triangleq \langle \mathbf{S}^2 \rangle$. Plotting these quantities against J, as in Fig. 10, provides an illuminating illustration of the linear growth in L within both bands, along with the near constant S_p, S_n, and S, and the shift between aligned and antialigned coupling for the two bands. Observe that the total spin ($S \approx 1/2$) comes primarily from the neutron spin ($S_n \approx 1/2$), with the proton spins coupling to give a total near zero ($S_p \approx 0$).[7]

A natural simple interpretation, based on this LS structure, identifies the two negative parity bands in ^{9}Be as LS spin-flip partners, involving the same orbital (that is, spatial) structure but opposite couplings to the spin [16]. The orbital motion is then consistent with being rotational in nature, described by a $K_L = 1$ band with orbital angular momenta $L = 1, \ldots, 4$. That

[4] In the context of the shell model, where the strength of the spin-orbit interaction controls the transition from LS to jj coupling, these schemes are termed the *weak coupling* and *strong coupling* regimes, respectively [62].

[5] The Lanczos trick, originally devised for evaluating strength functions [64–66], may be used to obtain the decomposition of a wave function with respect to eigenstates of any given Hermitian observable operator, such as the squared angular momentum operators, to obtain angular momentum decompositions [18], or a more general group's Casimir operator, to obtain a decomposition into irreps of this group [67]. It is necessary only to take the calculated wave function and use it as the new pivot vector for a Lanczos diagonalization of the $\mathbf{L}^2$ operator, $\mathbf{S}^2$ operator, or other operator of interest.

[6] The expectation value of $\langle \mathbf{L}^2 \rangle$, and thus the effective $\bar{L}$, can always be recovered from the full angular momentum decomposition by L, and thus provides no new information relative to this full decomposition (and similarly for the effective spin angular momenta). However, $\langle \mathbf{L}^2 \rangle$ is the expectation value of a rotational scalar two-body operator, a standard class of observables to extract from NCCI wave functions, and can be computed much more efficiently than the full decomposition, which requires further Lanczos diagonalizations.

[7] When interpreting small values of $\bar{L}$ or $\bar{S}$, we must keep in mind the nonlinear relationship entering into the definition of the effective angular momentum. A small admixture of higher spin into an $S = 0$ state can have an outsized effect on $\bar{S}$, *e.g.*, an effective $\bar{S} \approx 0.2$ is obtained with only a 10% admixture of $S = 1$.

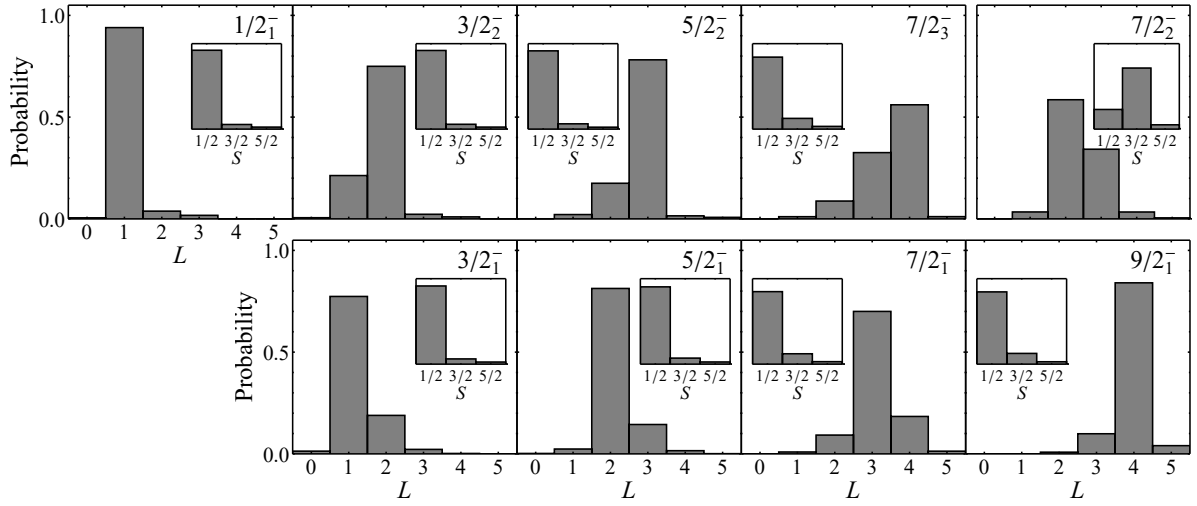

Fig. 9 Orbital angular momentum decompositions of ^{9}Be negative parity states: $K^P = 3/2^-$ ground state band members ($3/2^-_1$, $5/2^-_1$, $7/2^-_1$, $9/2^-_1$) (bottom), $K^P = 1/2^-$ excited band members ($1/2^-_1$, $3/2^-_2$, $5/2^-_2$, and $7/2^-_3$) (top left), and an off-yrast state lying between the bands ($7/2^-_2$) (top right). Spin angular momentum decompositions are shown as insets. Based on wave functions calculated for $N_{\max} = 10$.

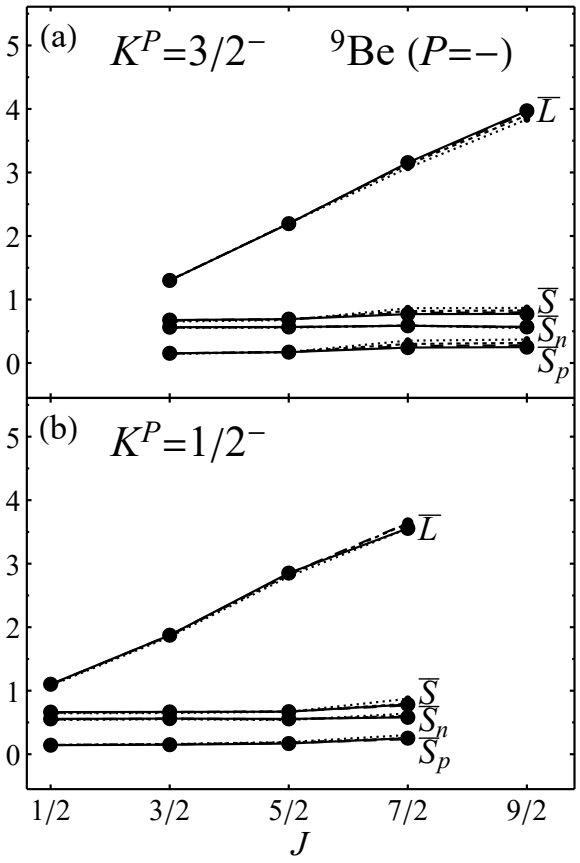

Fig. 10 Effective values of orbital and spin angular momenta for ^{9}Be negative parity rotational band members: (a) $K^P = 3/2^-$ ground state band and (b) $K^P = 1/2^-$ excited band. Based on wave functions calculated for $N_{\max} = 4$ to 10 (dotted through solid curves).

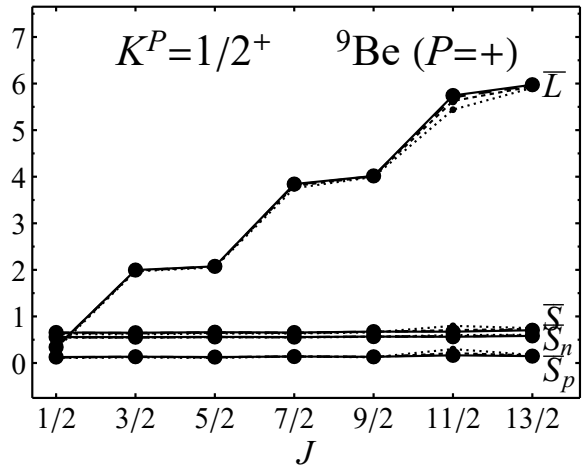

Fig. 11 Effective values of orbital and spin angular momenta for ^{9}Be positive parity rotational band members ($K^P = 1/2^+$ band). Based on wave functions calculated for $N_{\max} = 5$ to 11 (dotted through solid curves).

is, the orbital motion is based on an intrinsic state with projection $K_L = 1$ of the orbital angular momentum along the symmetry axis. In this limit of the rotational interpretation, based on weak coupling of spin to spatial rotation,[8] the total angular momenta

[8] Here we encounter the terminology of weak *vs.* strong coupling now in the sense not of shell model angular momentum coupling schemes (footnote 4) but rather of collective motion, in which the nucleus is presumed to factorize into a collective core and residual degrees of freedom, typically the last odd "uncoupled" nucleon (see Sec. 1.8 of Ref. [5] and Sec. 7.5 of Ref. [50]). In weak coupling, the residual degree of freedom (in the present example, the last unpaired neutron spin), only

$J = 1/2, 3/2^2, 5/2^2, 7/2^2, 9/2$ then follow simply by angular momentum coupling of L and S.

For the positive parity band ($K^P = 1/2^+$), a decidedly different LS angular momentum structure is obtained, as may be seen from the effective angular momenta in Fig. 11. Here, the spin is again predominantly $S \approx 1/2$ and again arises from the neutrons, but the orbital angular momenta now form a stair-step pattern: $L \approx 0, 2, 2, 4, 4, 6, 6$, for the $J = 1/2, \ldots, 13/2$ states, respectively. A natural simple description for this band is thus based on orbital motion consisting of a $K_L = 0$ rotational band, containing even values of angular momentum ($L = 0, \ldots, 6$). Then, successive band members alternate between anti-aligned and aligned couplings of L and S.

We have already noted that the negative parity band members in the *ab initio* calculations appear to be primarily $0\hbar\omega$ states (Sec. 3.2) and could thus potentially be described within a shell-model effective theory. It is thus informative to compare their LS momentum structure with that expected in an Elliott SU(3) shell model description. The states which are brought lowest in energy by an SU(3) quadrupole-quadrupole Hamiltonian are those forming the leading irrep of SU(3) arising in the valence shell model space of the nucleus, *i.e.*, the irrep having the largest eigenvalue for the SU(3) Casimir operator. For ^{9}Be, the leading irrep has quantum numbers $(\lambda, \mu) = (3, 1)$ and, from fermionic antisymmetry constraints, occurs in association with a total spin $S = 1/2$. According to the SU(3) $\rightarrow$ SO(3) angular momentum branching rule, the $(3, 1)$ irrep indeed contains a single $K_L = 1$ band, with $L = 1, 2, 3, 4$, exactly as found here in the *ab initio* calculations.

While we have focused thus far on the strict LS weak coupling limit (in the both the shell model and collective model senses of weak coupling), such does not provide a satisfactory description beyond reproducing the overall angular momentum J content of the bands. Indeed, the simple picture of a K_L band, with rotation only in the orbital degrees of freedom, would give an energy spacing proportional to $L(L + 1)$ rather than $J(J + 1)$, as seen in Fig. 1, and sets aside the question of the Coriolis staggering.

However, as demonstrated by Elliott and Wilsdon [38] in the SU(3) picture, a modest spin-orbit interaction (intermediate coupling, in the shell model sense) serves to mix the states of different L but coupled with spin to give the same final J (*i.e.*, $L = J \pm 1/2$) arising from the two spin-flip partner bands or, more generally, within the same SU(3) irrep. The resulting spectrum consists of states which approximate a conventional rotational spectrum, with states of definite $K = K_L + K_S$ (strong coupling, in the collective rotational sense) as in (1) and following the rotational energy formula (2) or (3). The resulting SU(3) interpretation of the ^{9}Be ground state band, including mixing, is discussed by Millener [68]. Certainly, some such L mixing ($L = J \pm 1/2$) is apparent for the calculated states in Fig. 9.

While weak coupling (good L) states form an orthogonal basis, the strong rotational coupling (good K) states obtained within a shell model space, in the Elliott-Wilsdon picture, lead to a breakdown of the band structure at high J, *i.e.*, near band termination. The resulting state in the SU(3) shell model picture cannot be uniquely identified with a specific K band (recall the ambiguous transition pattern from the terminating $9/2^-$ state in Sec. 3.1).

The orbital angular momentum projections K_L for the rotational intrinsic state suggested by these observations on the LS structure of ^{9}Be are also consistent with the appealing intuitive description of these bands as arising from nuclear molecular rotation. In a molecular description, ^{9}Be is composed of two α clusters plus a single valence neutron, which occupies a molecular orbital in the potential generated by the clusters [69–72]. Within each α particle, the spins of both protons and of both neutrons must couple to give zero resultant spin, leaving only the spin contribution of the last neutron ($S = 1/2$). Thus, while the rotational band members in the negative parity space could be consistent with such a picture, other low-lying states, *e.g.*, the calculated $7/2^-_2$ state, with dominant spin contribution $S = 3/2$ [Fig. 9 (top right)], must involve breaking of an α particle.

In the phenomenological cluster molecular orbital description, as discussed in Ref. [72], both the $K^P = 3/2^-$ and $K^P = 1/2^-$ negative parity bands are obtained from an intrinsic state in which the neutron is in a π orbital, *i.e.*, giving angular momentum projection $K_L = 1$ along the symmetry axis defined by the clusters. Rotational strong-coupling intrinsic states with definite $K = 3/2$ and $K = 1/2$ then arise from the aligned and anti-aligned combinations $K = K_L \pm K_S$, respectively, with the projection $K_S = 1/2$ of the neutron spin along the symmetry axis. The positive parity $K^P = 1/2^+$ band instead arises from an intrinsic state for which the neutron is in a σ orbital, *i.e.*, giving $K_L = 0$, and thus $K = K_S = 1/2$.

combines with the collective motion through angular momentum coupling to yield the total angular momentum of the system, while, in strong coupling, the nominally residual degree of freedom in fact fully participates in the intrinsic wave function $|\phi_K\rangle$. Thus the adiabatic rotational wave function described in (1) represents the strong coupling limit of collective rotation.

4 ^{11}Be: Rotation outside the valence space

4.1 Rotational spectrum and convergence

The low-lying calculated spectrum of ^{11}Be, shown in Fig. 2, brings in new rotational characteristics, most notably, a natural parity rotational band which lies outside the realm of a $0\hbar\omega$ effective theory. These rotational bands again have well-defined angular momentum structures in an LS coupling picture.

The nucleus ^{11}Be is well-known for the so-called parity inversion which arises in the spectrum. That is, the experimental $1/2^+$ ground state is of positive (and thus unnatural) parity, contrary to what might naively be expected from shell-model considerations [73]. It lies 0.320 MeV below the $1/2^-$ lowest negative (natural) parity level [57]. This parity inversion, which is generally considered challenging to reproduce in an *ab initio* NCCI framework and known to be sensitive to the details of the interaction [74, 75], is obtained in calculations with the Daejeon16 interaction [76]. Considering the near degeneracy of the lowest $0\hbar\omega$ and $1\hbar\omega$ states, within a shell-model interpretation, it is perhaps not surprising that $2\hbar\omega$ states should also be found at low excitation energy.

Starting with the negative parity spectrum, the calculated $1/2^-_1$, $3/2^-_1$, $5/2^-_1$, and $7/2^-_2$ states [Fig. 2(a)] may be identified as forming a $K^P = 1/2^-$ band. The angular momenta in the negative parity ground state band extend to the maximal angular momentum $J = 7/2$ which can be constructed in the valence ($0\hbar\omega$) space. The $E2$ transitions follow the characteristic transition pattern for a $K = 1/2$ band (Fig. 5). There is modest positive Coriolis staggering ($a \approx 0.4$). We shall refer to this band, in the following discussion, as the "negative parity ground state band", in that it is built on the ground state of the negative parity space, in distinction to the "positive parity ground state band", built on the ground state of the positive parity space (which becomes the overall ground state both in the high $N_{\max}$ calculations here and in experiment).

However, there are also enhanced $E2$ connections from the negative parity ground state band to the $3/2^-_3$ and $5/2^-_3$ states. These states are themselves connected by a strong $E2$ transition, comparable to the in-band transitions, suggesting that these states could be described as constituting a $K^P = 3/2^-$ band, albeit a very short one, which would spectroscopically be described as a side band to the negative parity ground state band.

Then, threading between these bands in energy [Fig. 2(a)], is another $K^P = 3/2^-$ band. This band becomes yrast at $J = 7/2$, and then extends through this maximal valence angular momentum with no noticeable disruption to the rotational energies, finally terminating at $J = 13/2$. In comparison with the "short" negative parity ground state band ($A \approx 0.6$ MeV), this "long" band has energies which follow a line with a significantly shallower slope ($A \approx 0.3$ MeV). Between the short band and the long band, there is thus an approximate doubling of the moment of inertia. The long band does not have significant $E2$ connections to the short bands.

Considerations of convergence are especially important for the $K^P = 3/2^-$ long band. The excitation energies of the negative parity band members at various $N_{\max}$ are traced out in Fig. 12. The long band starts at high excitation energy in the spectrum, at low $N_{\max}$, but rapidly descends with increasing $N_{\max}$. For instance, the $7/2^-$ band member only becomes yrast at $N_{\max} = 8$. The low final energy for the long band in the present calculations with the Daejeon16 interaction, at the highest $N_{\max}$ considered here ($N_{\max} = 10$), reflects the comparatively rapid convergence obtained with the Daejeon16 interaction. In comparison, in calculations with the JISP16 or NNLO$_{\rm opt}$ interactions, at this same $N_{\max}$, the band head energy still lies well above 10 MeV [14, 16, 29]. Without attempting any detailed extrapolation here, we can observe that the calculated energies of the long band members appear to be converging towards those of a corresponding experimentally identified excited rotational band [58, 59] (see Refs. [29, 30] for further discussion of and comparison with the experimental levels and rotational energy parameters).

Within the positive parity spectrum [Fig. 2(b)], the yrast and near-yrast states can likewise be identified as forming rotational bands, based on energies and enhanced $E2$ connections. The $K^P = 1/2^+$ positive parity ground state band terminates at $J = 9/2$, and exhibits large positive Coriolis staggering ($a \approx 1.9$). (Note the excellent agreement of the *ab initio* predicted excitation energies within the band for the lowest three band members with experimentally observed levels.) Next lies an excited $K^P = 5/2^+$ band, which becomes yrast at $J = 11/2$ and terminates at $J = 13/2$, the maximal angular momentum accessible in the $1\hbar\omega$ space. The moments of inertia of these bands differ (the slope parameter is $A \approx 0.4$ MeV for the $K^P = 1/2^+$ band and $A \approx 0.25$ MeV for the $K^P = 5/2^+$ band).

There are some modestly enhanced $E2$ transistions between these bands and to other low-lying states (namely, $3/2^+_2$ and $5/2^+_3$). Most noticeable, though, is the $E2$ transition pattern from the terminating $13/2^+$ state, which is at the maximal angular momentum accessible in the $1\hbar\omega$ space. Although the energy of this

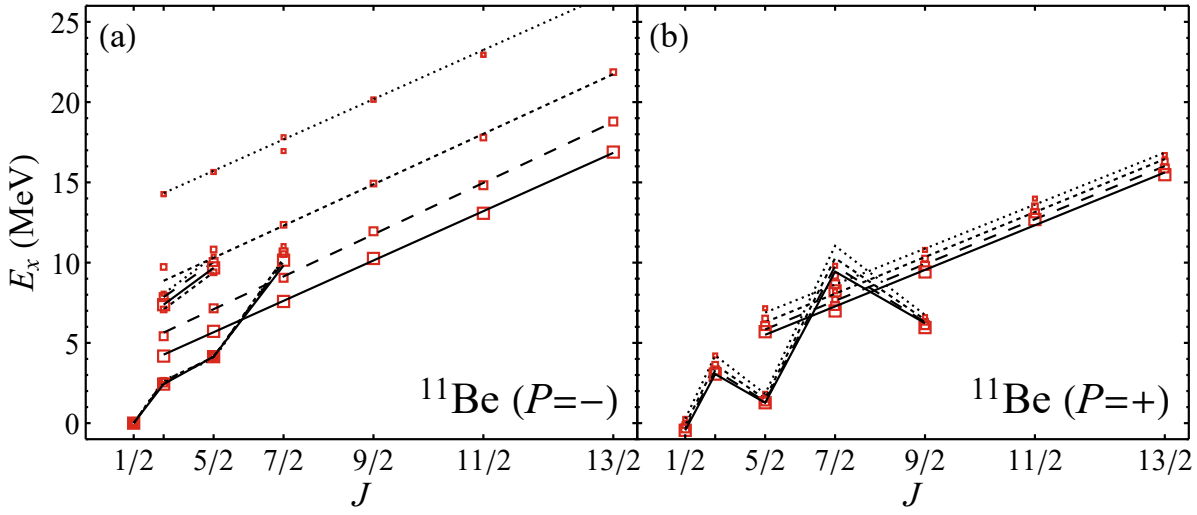

Fig. 12 Calculated energies for rotational band members in ^{11}Be, for (a) negative and (b) positive parity, shown as excitation energies relative to the negative parity ground state. The calculated bands are for $N_{\max} = 4$ to 10 or $N_{\max} = 5$ to 11, respectively (dotted through solid curves).

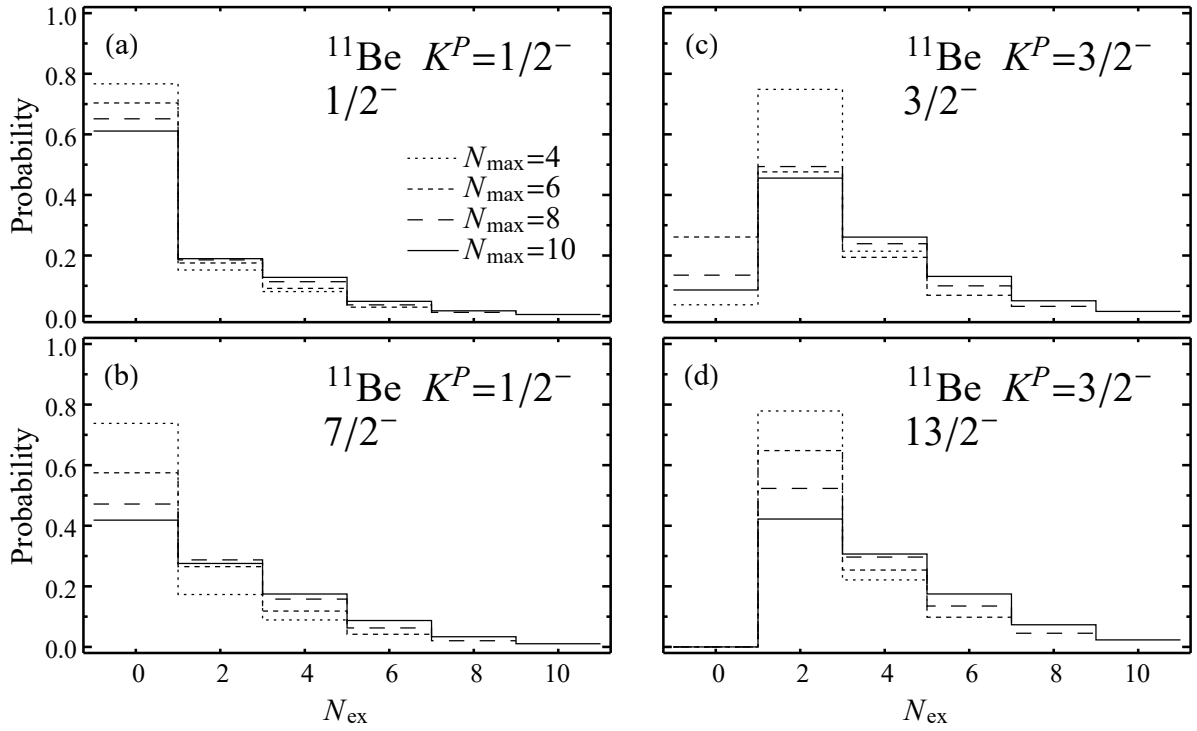

Fig. 13 Decompositions of representative ^{11}Be negative parity rotational band members: (Left) The $K^P = 1/2^-$ negative parity ground state band's (a) $1/2^-$ band head and (b) $7/2^-$ terminating state. (Right) The $K^P = 3/2^-$ negative parity long band's (c) $3/2^-$ band head and (d) $13/2^-$ terminating state. Decompositions are calculated from wave functions obtained for $N_{\max} = 4$ to 10 (dotted through solid curves).

state is roughly consistent with membership in the $K^P = 5/2^+$ band, the strongest $E2$ transition is to the $K^P = 1/2^+$ band, suggesting a breakdown of the rotational strong coupling picture at high J (recall the termination effects from Sec. 3.3).

4.2 Structure in oscillator space

The levels in the negative parity ground state band have largest contributions coming from $0\hbar\omega$ oscillator configurations, as may be seen for representative band mem-

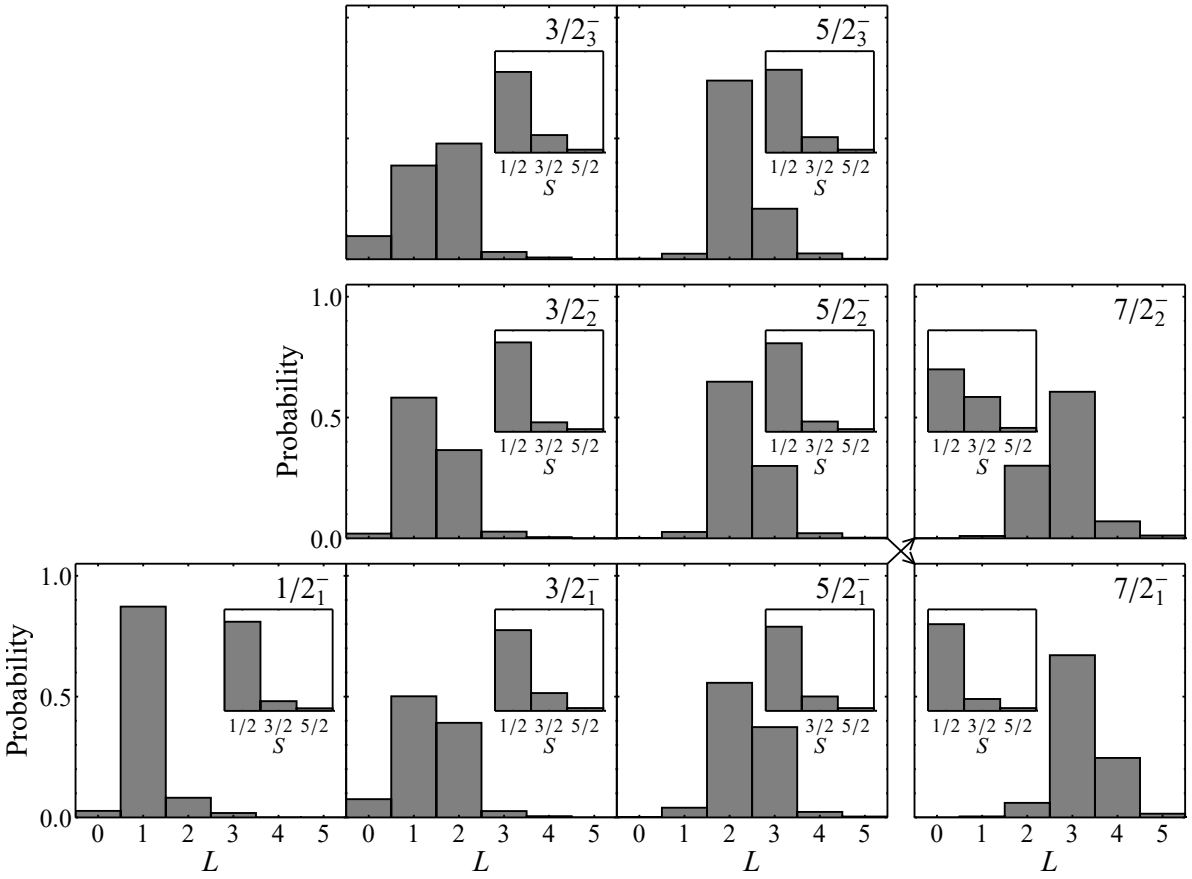

Fig. 14 Orbital angular momentum decompositions of ^{11}Be negative parity states: $K^P = 1/2^-$ negative parity ground state band members ($1/2^-_1$, $3/2^-_1$, $5/2^-_1$, and $7/2^-_2$) (bottom), $K^P = 3/2^-$ long band members ($3/2^-_2$, $5/2^-_2$, and $7/2^-_1$) (middle), and $K^P = 3/2^-$ side band members ($3/2^-_3$ and $5/2^-_3$) (top). The crossed arrows indicate the change in energy ordering of the first two bands between $J = 5/2$ and $7/2$. Spin angular momentum decompositions are shown as insets. Based on wave functions calculated for $N_{\max} = 10$.

bers in Fig. 13(a,b). The members of the $K^P = 3/2^-$ side band have similar decompositions.

However, for the states constituting the $K^P = 3/2^-$ long band, a qualitatively different oscillator decomposition is obtained [Fig. 13(c,d)]. While band members with angular momenta above the maximal valence angular momentum ($J = 7/2$) cannot receive any contribution from $0\hbar\omega$ oscillator basis configurations [Fig. 13(d)], even for those band members lying beneath the maximum valence angular momentum the $0\hbar\omega$ contribution is highly suppressed [Fig. 13(c)], as initially noted in Ref. [30]. The largest contribution comes from $2\hbar\omega$ basis states, after which the probability distribution falls off gradually for higher $N_{\rm ex}$.

4.3 Angular momentum structure

The states making up the rotational bands in ^{11}Be, like those in ^{9}Be, again follow comparatively simple patterns when viewed in terms of an LS coupling scheme, as indicated by their LS decompositions, as shown in Fig. 14, or, again, more simply in terms of the evolution of the effective $\bar{L}$ and $\bar{S}$ values as functions of J within the band, as shown in Figs. 15 and 16. For all these bands in ^{11}Be, the predominant total spin $S = 1/2$ arises from the neutrons ($S_n = 1/2$), while the proton spin vanishes ($S_p = 0$).

For the $K^P = 3/2^-$ long band [Fig. 14 (middle)], the angular momentum structure is comparatively straightforward. The $J = 3/2, \ldots, 13/2$ band members have orbital angular momenta of predominantly $L = 1, \ldots, 6$, respectively. The simple linear growth in L with J may be seen most clearly in Fig. 15(c). Thus, the orbital motion is consistent with a band built on an $K_L = 1$ state for intrinsic motion, which then combines with the total spin $S = 1/2$ in aligned coupling to give $J = L + 1/2$.

For the $K^P = 1/2^-$ negative parity ground state band and $K^P = 3/2^-$ side band, if we simply examine the effective $\bar{L}$ values [Fig. 15(a,b)], the pattern is less obvious. However, from the detailed angular mo-

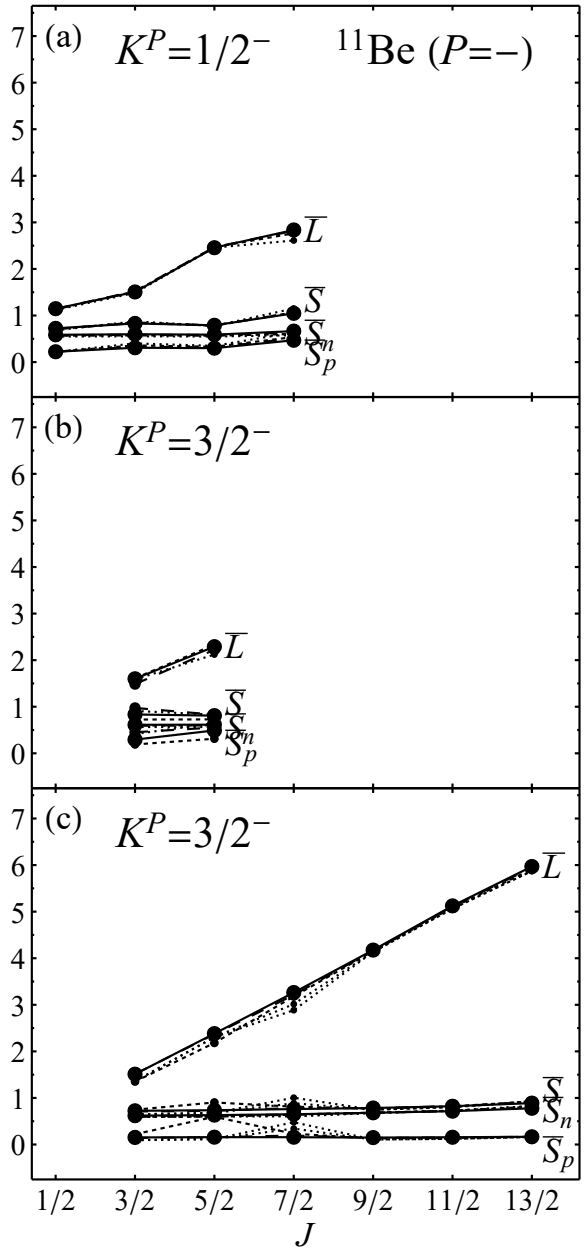

Fig. 15 Effective values of angular momenta for ^{11}Be negative parity rotational band members: (a) $K^P = 1/2^-$ negative parity ground state band, (b) $K^P = 3/2^-$ negative parity side band, and (c) $K^P = 3/2^-$ negative parity long band. Based on wave functions calculated for $N_{\max} = 4$ to 10 (dotted through solid curves).

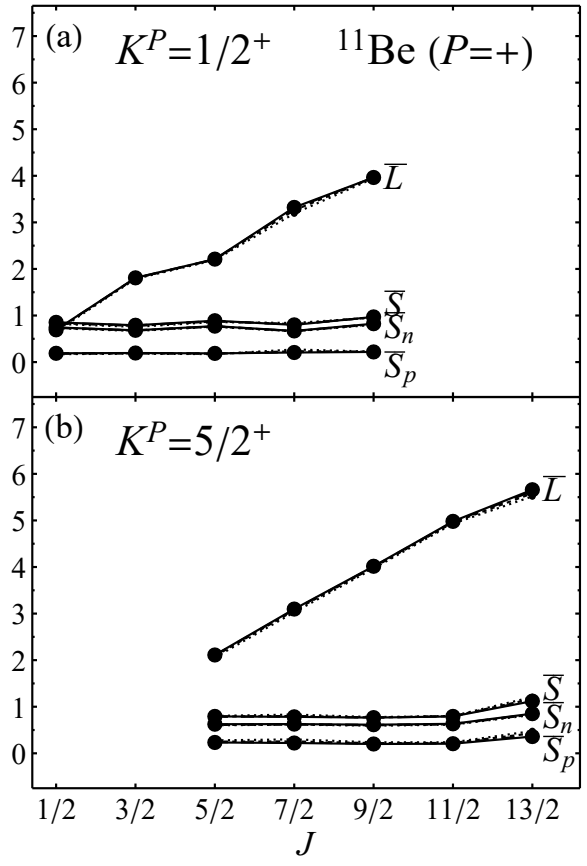

Fig. 16 Effective values of angular momenta for ^{11}Be positive parity rotational band members: (a) $K^P = 1/2^+$ positive parity ground state band and (b) $K^P = 5/2^+$ positive parity excited band. Based on wave functions calculated for $N_{\max} = 5$ to 11 (dotted through solid curves).

mentum decompositions [Fig. 14 (bottom,top)], it becomes clear that the contributing orbital angular momenta are $L = 1, 2, 3$. The total set of angular momenta ($J = 1/2, 3/2^2, 5/2^2, 7/2$) constituting the negative parity ground state band and its side band are consistent with a single $K_L = 1$ rotational band in the orbital motion, with $L = 1, 2, 3$, combining with the spin in antialigned ($J = 1/2, 3/2, 5/2$) and aligned ($J = 3/2, 5/2, 7/2$) couplings. However, here there is clearly much stronger mixing between the states of same J but different L than in the two negative parity bands in ^{9}Be, for which the angular momentum decompositions more cleanly indicate the aligned and antialigned couplings of a single $K_L = 1$ band with $S = 1/2$.

Suggestively, the angular momentum structure for these negative parity ground state and side bands is again exactly as expected from a simple Elliott SU(3) picture, as described by Millener [68]. For ^{11}Be, the leading irrep has $(\lambda, \mu) = (2, 1)$ and arises with $S = 1/2$. By the SU(3) $\rightarrow$ SO(3) angular momentum branching rule, this irrep indeed contains a single $K_L = 1$ band with $L = 1, 2, 3$, giving rise to $K = 1/2$ and $3/2$ bands.

For the positive parity ground state band ($K^P = 1/2^+$) [Fig. 16(a)], the orbital motion is described by a $K_L = 0$ band comprised of even angular momenta, much as for the postive parity band of ^{9}Be, but here terminating at $L = 4$ ($L = 0, 2, 4$). These orbital angular momenta again couple alternately in antialigned

and aligned couplings with the spin $S = 1/2$ to give $J = 1/2, \ldots, 9/2$.

Then, for the positive parity excited band ($K^P = 5/2^+$) [Fig. 16(b)], we now seem to find a $K_L = 2$ orbital motion, with $L = 2, 3, 4, 5, 6$. These orbital angular momenta combine in aligned coupling with the spin ($S = 1/2$) to give $J = 5/2, \ldots, 13/2$. (Ostensibly a band arising from the antialigned coupling might be found at higher excitation energy.)

Note that the spin structure ($S = 1/2$ from neutrons) found in the calculated rotational bands is again consistent with alpha cluster molecular structure. In the molecular description of ^{11}Be, the proton spins are coupled pairwise to zero, within alpha particles, as are the spins of the neutrons within the alpha particles. The total spin thus arises from the three valence neutrons, and ostensibly just the last unpaired valence neutron.

It is then perhaps reassuring that organization of the structure into rotational bands for the orbital motion, with the K_L values suggested by the present interpretation of the *ab initio* calculations, is generally consistent with the description obtained in antisymmetrized molecular dynamics (AMD) calculations for ^{11}Be, in terms of cluster molecular orbitals (see Sec. 3.1.2 of Ref. [77]). That is, the negative parity ground state band ($K^P = 1/2^-$) is based on a π^3 configuration, and the long band ($K^P = 3/2^-$) is based on a $\pi\sigma^2$ configuration, consistent with $K_L = 1$ from an unpaired neutron in a π orbital. Then, the lowest positive parity band ($K = 1/2$) in the AMD description is based on a $\pi^2\sigma$ configuration, consistent with $K_L = 0$ from destructive addition of $K_L = \pm 1$ contributions from the two paired π orbitals (it is also natural to obtain $K_L = 2$, from constructive addition, as found here for the $K^P = 5/2^+$ excited band).

5 ^{7}Be: Quadrupole excitation

5.1 Rotational spectrum and discussion

The rotational structure emerging in the *ab initio* calculations for ^{7}Be, as shown in Fig. 3, shares some of the characteristics we have just explored for ^{9}Be and ^{11}Be. However, it also hints at the emergence of further effective degrees of freedom. In particular, it demonstrates the relevance of quadrupole degrees of freedom and indicates a richer role for dynamical symmetry as an organizing scheme for collective excitations.

The calculated negative parity spectrum (Fig. 3) contains a $K^P = 1/2^-$ ground state band, which terminates the maximal valence angular momentum ($J = 7/2$) for ^{7}Be. The staggering of energies in this band is of the type obtained for a negative value of the Coriolis decoupling parameter a (that is, the $J = 1/2, 5/2, \ldots$ members are raised and $J = 3/2, 7/2, \ldots$ members lowered, contrary to the other $K = 1/2$ bands discussed above). Indeed, this staggering is sufficiently pronounced that the $3/2^-$ band member becomes the ground state, both in the calculations and in experiment.

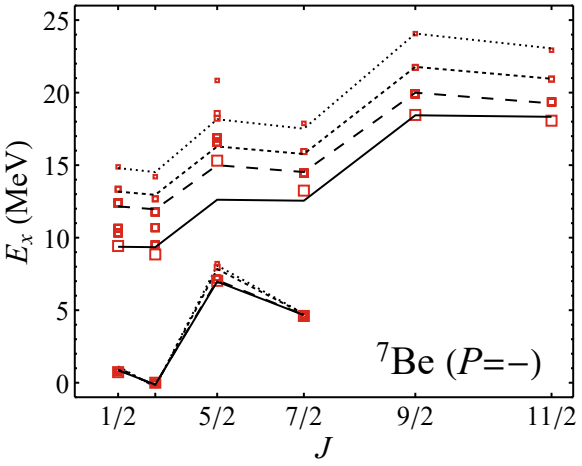

Fig. 17 Calculated energies for ^{7}Be rotational band members, shown as excitation energies relative to the negative parity ground state. The calculated bands are for $N_{\max} = 8$ to 14 (dotted through solid curves).

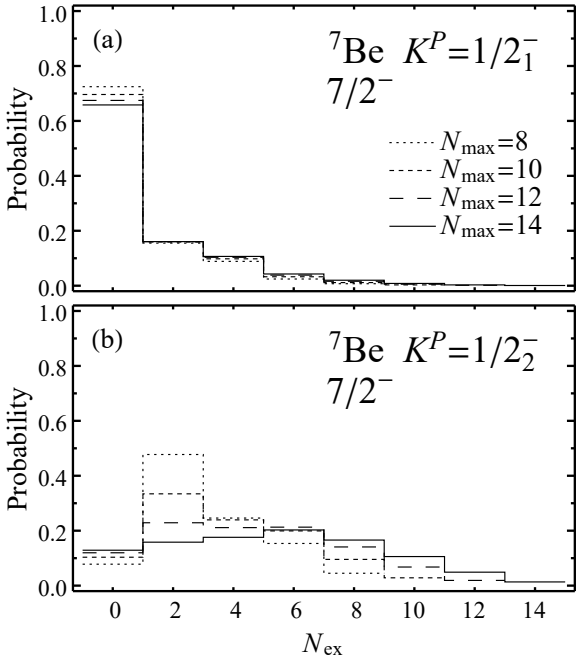

Fig. 18 Decompositions of representative ^{7}Be negative parity rotational band members: (a) the $K^P = 1/2^-$ ground state band's $7/2^-$ terminating state and (b) the $K^P = 1/2^-$ excited band's $7/2^-$ member. Decompositions are calculated from wave functions obtained for $N_{\max} = 8$ to 14 (dotted through solid curves).

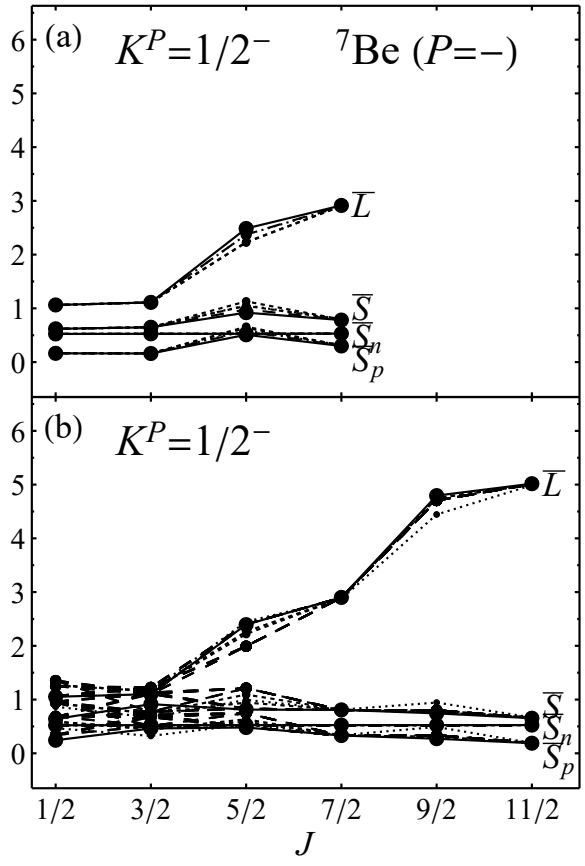

Fig. 19 Effective values of orbital and spin angular momenta ($\bar{L}$, $\bar{S}_p$, $\bar{S}_n$, and $\bar{S}$, as labeled) for ^{7}Be rotational band members: (a) $K^P = 1/2^-$ ground state band and (b) $K^P = 1/2^-$ excited band. Based on wave functions calculated for $N_{\max} = 8$ to 14 (dotted through solid curves).

The $5/2^-$ band member, which is staggered upwards in energy, forms a close doublet with another, apparently non-rotational $5/2^-$ state. As the calculated energies evolve with the basis truncation $N_{\max}$, the $5/2^-$ member of the ground state band begins slightly above the non-rotational $5/2^-$ state, in low-$N_{\max}$ calculations, and then ends up at lower energy, in high-$N_{\max}$ calculations. The crossing occurs at $N_{\max} = 10$, at which point the $E2$ strengths indicate significant two-state mixing. Note that a close $5/2^-$ doublet is observed experimentally as well (Fig. 3). (With the exception of this $5/2^-$ band member, the calculated excitation energies within the ground state band are seen to be essentially independent of $N_{\max}$ in Fig. 17.)

The calculated wave functions for the ground state band members are predominantly $0\hbar\omega$ in character, as illustrated for the terminating $7/2^-$ band member in Fig. 18(a). Moreover, inspection of the angular momenta, in Fig. 19(a), indicates once again a straightforward angular momentum structure in the LS scheme. The spin is predominantly $S \approx 1/2$ (and arises from the neutrons). The orbital angular momenta again form a stair-step pattern, as for the positive parity $K = 1/2$ band in ^{9}Be (recall Fig. 11), but now with odd values for L, namely, $L = 1, 1, 3, 3$, for the $J = 1/2, \ldots, 7/2$ states, respectively. The angular momentum content of the $5/2^-$ band member is perturbed by two-state mixing with the nearby non-rotational $5/2^-$ state, which has major contributions with $S_p = 1$ and $S = 3/2$, especially at their closest approach in energy ($N_{\max} = 10$).

Due to basic symmetry considerations, a $K = 0$ rotational band may contain either only even angular momenta or only odd angular momenta, depending whether the intrinsic wave function takes on a positive or negative sign ($r = \pm 1$) under a rotation of π around an axis perpendicular to the symmetry axis, respectively [50, 78]. Thus, the angular momentum structure of the ground state band in ^{7}Be is consistent with an orbital motion described by a $K_L = 0$, $r = -1$ rotational band, containing odd values of angular momentum ($L = 1, 3$), which then combine alternately in antialigned and aligned coupling with the spin ($S = 1/2$) to give successive band members.

Such a picture has, in fact, long been speculated from a cluster molecular orbital description, in which ^{7}Be may be viewed as two α particles plus a neutron hole occupying a σ molecular orbital. See the discussion (of the mirror nuclide ^{7}Li) in Sec. 10 of Ref. [62], where it is, in particular, suggested that the ground state $3/2^-$ and first excited $1/2^-$ states are obtained from the aligned and antialigned couplings, respectively, of the same $K_L = 0$, $L = 1$ motion to spin ($S = 1/2$). In the limit of large cluster separations, this molecular orbital description reduces to removal of a neutron from one α to form an α-^{3}He molecule (here it may be helpful to refer to a molecular orbital diagram, as in Fig. 5 of Ref. [72]).

If we now look beyond the maximal valence angular momentum in Fig. 3, there is a puzzling feature to the spectrum. One particular $9/2^-$ state, slightly above the yrast line, and the yrast $11/2^-$ state have strong $\Delta J = 2$ $E2$ transitions to the $5/2^-$ and $7/2^-$ ground state band members, respectively. Indeed, these transitions are comparable in strength to in-band transitions.

On the one hand, such enhanced transitions could suggest that these $9/2^-$ and $11/2^-$ states might be taken as possible ground state band members, as discussed in Refs. [13, 14, 16]. The calculated energies lie high relative to what we would expect for $J = 9/2$ and $11/2$ band members, based on the rotional energy formula (3), but the excitation energies are not well converged and are still decreasing with $N_{\max}$, so such a comparison is ambiguous.

On the other hand, these $9/2^-$ and $11/2^-$ states also have $\Delta J = 2$ transitions, of comparable strength, to specific higher-lying $5/2^-$ and $7/2^-$ states, respectively. Indeed, in the present calculations, we can trace out a complete excited $K^P = 1/2^-$ band from the $E2$ strengths, terminating with these yrast $9/2^-$ and $11/2^-$ states (Fig. 3).[9] Thus, the transitions from these $9/2^-$ and $11/2^-$ states to the ground state band members are not in-band transitions, but rather highly enhanced interband $E2$ transitions.

In a calculation at any given $N_{\max}$, such as the $N_{\max} = 14$ calculation in Fig. 3, individual band members, especially the upward-staggered states ($J = 1/2, 5/2, 9/2$), are subject to transient two-state mixing with other "background" states, due to accidental degeneracies in energy (see Sec. IV A of Ref. [14]). This complication will tend to somewhat obscure any investigation of the properties of the band members, but the basic features are apparent.

In particular, the excited band members, whether above the maximal valence angular momentum or below, have their largest contributions coming from $2\hbar\omega$ or higher oscillator contributions, as shown in Fig. 18(b). At modest $N_{\max}$ values, the decomposition is sharply peaked at $2\hbar\omega$, but the distribution becomes much broader for the highest $N_{\max}$ calculations, peaking at $4\hbar\omega$ or even $6\hbar\omega$ contributions.

Then, the orbital angular momenta, in Fig. 19(b), follow the same stair-step pattern as for the ground state band, consistent with a $K_L = 0$ rotational motion restricted to odd L ($r = -1$), but now extending to $L = 5$. (The upward-staggered $J = 1/2, 5/2, 9/2$ band members, and the lower J band members in general, are more subject to transient contamination of their angular momentum content from mixing at specific $N_{\max}$ values.)

Although transient mixing or fragmentation makes it difficult to accurately track the convergence of the excitation energies of the lower-J band members with increasing $N_{\max}$, this convergence is indicated to the extent possible in Fig. 17. At least superficially, the excited $K^P = 1/2^-$ band in ^{7}Be would seem to resemble the long $K^P = 3/2^-$ band in ^{11}Be, which similarly receives predominant contributions from $2\hbar\omega$ or higher configurations and extends beyond the maximal valence angular momentum (Sec. 4.1). The calculated excitation energies for both bands move rapidly downward with increasing $N_{\max}$ [compare Fig. 12(a) for ^{11}Be and Fig. 17 for ^{7}Be].

However, there are also notable differences in the convergence properties. In particular, the long band in ^{11}Be seems to be rapidly approaching a final, converged excitation energy (with each successive step in $N_{\max}$, the change in excitation energy is smaller by about half). In contrast, the convergence pattern of the energies of the excited band in ^{7}Be is still not clearly defined.

[9] A hint of the excited band structure may already be found in Fig. 10 of Ref. [16], where enhanced transitions may be seen from the yrast $9/2^-$ and $11/2^-$ states to high-lying $5/2^-$ and $7/2^-$ states. However, the calculations of Refs. [13–16] were based on the less rapidly convergent JISP16 and $\mathrm{NNLO_{opt}}$ interactions, and only carried to $N_{\max} = 10$, so the excited band members lay at higher excitation energy, obscured in a region of higher level density, in these earlier calculations.

5.2 Dynamical symmetry structure

To understand the relationship between the ground state band and the excited band in the *ab initio* calculations for ^{7}Be, and how this might hint at the emergence of new effective theories, we turn to the symplectic group $\mathrm{Sp}(3,\mathbb{R})$ in three dimensions [39, 40, 79]. This group augments the generators of Elliott's U(3), which all conserve the total number of oscillator quanta, with further generators which physically represent the creation and annihilation operators for giant monopole and quadrupole resonances. These latter generators either create or destroy two oscillator quanta and can therefore connect $0\hbar\omega$ and $2\hbar\omega$ states. The giant quadrupole resonance operators in particular are naturally implicated if $0\hbar\omega$ and $2\hbar\omega$ states are connected by strong $E2$ transitions.

We are aided by calculations carried out in a symplectic no-core configuration interaction (SpNCCI) framework [47, 60, 80], in which the nuclear many-body basis is organized into irreps of the group chain

$$\left[\underset{\sigma}{\mathrm{Sp}(3,\mathbb{R})} \supset \underset{\omega}{\mathrm{U}(3)} \supset \underset{L}{\mathrm{SO}(3)}\right] \times \underset{S}{\mathrm{SU}_S(2)} \supset \underset{J}{\mathrm{SU}_J(2)}, \quad (6)$$

with quantum numbers as shown, where $\sigma \equiv N_{\sigma,\mathrm{ex}}(\lambda_\sigma, \mu_\sigma)$ and $\omega \equiv N_{\omega,\mathrm{ex}}(\lambda_\omega, \mu_\omega)$. It is then straightforward to extract the decomposition of the calculated wave functions not only with respect to the Elliott U(3) quantum numbers $N_{\omega,\mathrm{ex}}(\lambda_\omega, \mu_\omega)$, but the $\mathrm{Sp}(3,\mathbb{R})$ quantum numbers $N_{\sigma,\mathrm{ex}}(\lambda_\sigma, \mu_\sigma)$ as well. By way of explanation, we simply note here that a single $\mathrm{Sp}(3,\mathbb{R})$ irrep is obtained by starting from some "lowest" U(3) irrep σ, *i.e.*, having the lowest number of oscillator excitation quanta $N_{\sigma,\mathrm{ex}}$ within this particular $\mathrm{Sp}(3,\mathbb{R})$ irrep. Then the $\mathrm{Sp}(3,\mathbb{R})$ irrep consists of an infinite tower of U(3) irreps ω, *i.e.*, with $N_{\omega,\mathrm{ex}} = N_{\sigma,\mathrm{ex}}, N_{\sigma,\mathrm{ex}} + 2, \ldots$, obtained by laddering repeatedly with the giant resonance creation operators.

From calculations of ^{7}Be in a more restricted space ($N_{\max} = 6$), described in Refs. [47, 48], the U(3) structure of the bands becomes clear. The ground state band

members are identified with the $0\hbar\omega$ SU(3) irrep $(3,0)$, with $S = 1/2$, while the excited band members are identified with the $2\hbar\omega$ SU(3) irrep $(5,0)$, again with $S = 1/2$. The SU(3) $\rightarrow$ SO(3) angular momentum branching rule indeed yields that a $(3,0)$ irrep is comprised of a single $K_L = 0$ band with $L = 1, 3$, while a $(5,0)$ irrep is comprised of a single $K_L = 0$ band with $L = 1, 3, 5$. Thus, the $N_{\rm ex}$ and angular momentum structure detailed above for the rotational bands follows simply from an Elliott effective description.

Yet, it is also found that the U(3) irrep describing the excited band has a particular symplectic structure. The U(3) and spin quantum numbers $\omega S \equiv N_{\omega,\rm ex}(\lambda_\omega, \mu_\omega)S = 2(5,0)1/2$ are far from unique in the space for ^{7}Be, comprising a subspace of dimension 12. One (and only one) particular linear combination within this 12-dimensional space yields the U(3) irrep which is a member of the $\sigma S = N_{\sigma,\rm ex}(\lambda_\sigma, \mu_\sigma)S = 0(3,0)1/2$ symplectic irrep, that is, the symplectic irrep built on the ground state band's U(3) irrep by laddering with the giant resonance operators. And it turns out that the calculated excited band members lie within this symplectic irrep, at the level of $\sim 50\%$–80% of their norm.

Thus, the ground state and excited bands would seem to represent an example of approximate $\mathrm{Sp}(3,\mathbb{R}) \supset \mathrm{U}(3)$ dynamical symmetry. The strong interband $E2$ transitions reflect their connection by the giant quadrupole operator, which, as a generator of $\mathrm{Sp}(3,\mathbb{R})$, acts entirely within an $\mathrm{Sp}(3,\mathbb{R})$ irrep.

The dynamical symmetry relationship between the bands is suggestive of an emerging physical structure. In the contraction limit, obtained for large values of the quantum numbers, the microscopic symplectic picture gives way to a collective interpretation of the dynamics in terms of effective coupled rotational and vibrational (giant resonance) degrees of freedom [40, 41, 81, 82].

In such an extremely light and minimally bound nucleus as ^{7}Be, the physical interpretation is less clear. The contraction limit, essentially a semiclassical interpretation, is likely not well realized, and, when working within a bound state formalism as we are here, possible interactions with the scattering continuum could alter the interpretation of computed states. Nonetheless, at the very least, the emergence of rotational bands connected by quadrupole excitations in a symplectic dynamical symmetry scheme in these *ab initio* calculations may be taken as a possible harbinger of emergent rotational-vibrational structure in heavier and more strongly bound systems.

6 Conclusion

Microscopic *ab initio* theory offers the potential of predictive power, by addressing the nuclear many-body problem in its full glory, without presupposing mean-field structure, collective degrees of freedom, or many-body dynamical symmetries. It may therefore not be immediately obvious how to extract, from the results of such large-scale calculations, a physically intuitive understanding of the nucleus, of the kind afforded by models defined in terms of effective degrees of freedom. As has been said in the (slightly different) context of large-scale shell model calculations, "even if such calculations are possible using high-speed computers, the results are difficult to interpret physically and the consquences of agreement or disagreement with the data are much less intuitively informative... nor could one even begin to understand the resultant wave functions" [4].

Yet, *ab initio* theory has advanced to the point where the resulting calculated spectra do exhibit signatures of such emergent phenomena, including rotational features substantially resembling those observed in experiment. We see this in the present examples taken from the odd-mass Be isotopes (Figs. 1–3).

On one hand, most obviously, the calculated spectra may be taken in the spirit of a numerical experiment, permitting access to a rich set of observables in these nuclei, such as $E2$ strengths [83–86], which would otherwise be largely inaccessible due to experimental limitations. The traditional phenomenological analyis then takes over, starting from the computed "data", permitting the identification of emergent structural features. This is how collective features in the spectrum, such as rotational bands, are first identified.

On the other hand, the mere fact that the computed wave functions are "large" in an *ab initio* approach (for NCCI calculations, say, comprised of amplitudes for $\lesssim 10^{10}$ basis configurations) is in itself not an insurmountable impediment to discerning simple structure within these wave functions. The same large-scale computational tools which are used to generate the wave functions are also available to assist in their judicious analysis.

We have focused here on simple shell structure, which is hinted at by decompositions in oscillator space and band termination phenomena, and on simple angular momentum structure, which is apparent from LS decompositions [18]. These basic observations are consistent with and suggestive of a more complete understanding in terms of a richer structure of Elliott SU(3) and symplectic dynamical symmetries, as indicated both by the spectroscopy and by group theoretical decompositions of the wave functions [42–48, 60].

A complementary understanding [87] likely comes in terms of cluster molecular structure [9, 77]. For these light nuclei, where only a handful of lowest-energy states are truly bound, a more complete understanding requires going beyond a bound-state formalism towards approaches which can more directly identify clustering degrees of freedom underlying resonances [88, 89].

From these observations, we have provided some insight into the links between microscopic theory and emergent effective degrees of freedom, by recognizing basic structures and patterns in the *ab initio* results. The analyses presented here are essentially simple, focusing on spectroscopy and a few basic decompositions of the wave functions, but they already indicate the emergence of mean field structure, *LS* or intermediate-coupling rotation, and a nascent giant quadrupole degree of freedom.

Acknowledgements We thank Calvin W. Johnson and Tomáš Dytrych for valuable discussions. This material is based upon work supported by the U.S. Department of Energy, Office of Science, under Award Numbers DE-FG02-95ER-40934, DESC00018223 (SciDAC4/NUCLEI), and DE-FG02-87ER40371, and by the U.S. National Science Foundation under Award Number NSF-PHY05-52843. TRIUMF receives federal funding via a contribution agreement with the National Research Council of Canada. This research used computational resources of the University of Notre Dame Center for Research Computing and of the National Energy Research Scientific Computing Center (NERSC), a U.S. Department of Energy, Office of Science, user facility supported under Contract DE-AC02-05CH11231.

References

1. J.M. Eisenberg, W. Greiner, *Nuclear Theory*, vol. 1, 3rd edn. (North-Holland, Amsterdam, 1987)
2. F. Iachello, A. Arima, *The Interacting Boson Model* (Cambridge University Press, Cambridge, 1987)
3. I. Talmi, *Simple Models of Complex Nuclei: The Shell Model and Interacting Boson Model*, *Contemporary Concepts in Physics*, vol. 7 (Harwood Academic Publishers, Chur, Switzerland, 1993)
4. R.F. Casten, *Nuclear Structure from a Simple Perspective*, 2nd edn. No. 23 in Oxford Studies in Nuclear Physics (Oxford University Press, Oxford, 2000)
5. D.J. Rowe, J.L. Wood, *Fundamentals of Nuclear Models: Foundational Models* (World Scientific, Singapore, 2010)
6. T. Papenbrock, Nucl. Phys. A **852**, 36 (2011)
7. R.J. Furnstahl, Eur. Phys. J. A (this issue)
8. S.C. Pieper, R.B. Wiringa, J. Carlson, Phys. Rev. C **70**, 054325 (2004). DOI 10.1103/PhysRevC.70.054325
9. T. Neff, H. Feldmeier, Nucl. Phys. A **738**, 357 (2004). DOI 10.1016/j.nuclphysa.2004.04.061
10. P. Maris, J. Phys. Conf. Ser. **402**, 012031 (2012)
11. C. Romero-Redondo, S. Quaglioni, P. Navrátil, G. Hupin, Phys. Rev. Lett. **117**, 222501 (2016). DOI 10.1103/PhysRevLett.117.222501
12. P. Navrátil, S. Quaglioni, G. Hupin, C. Romero-Redondo, A. Calci, Physica Scripta **91**, 053002 (2016)
13. M.A. Caprio, P. Maris, J.P. Vary, Phys. Lett. B **719**, 179 (2013). DOI 10.1016/j.physletb.2012.12.064
14. P. Maris, M.A. Caprio, J.P. Vary, Phys. Rev. C **91**, 014310 (2015). DOI 10.1103/PhysRevC.91.014310
15. P. Maris, M.A. Caprio, J.P. Vary, Phys. Rev. C **99**, 029902(E) (2019). DOI 10.1103/PhysRevC.99.029902
16. M.A. Caprio, P. Maris, J.P. Vary, R. Smith, Int. J. Mod. Phys. E **24**, 1541002 (2015). DOI 10.1142/S0218301315410025
17. B.R. Barrett, P. Navrátil, J.P. Vary, Prog. Part. Nucl. Phys. **69**, 131 (2013). DOI 10.1016/j.ppnp.2012.10.003
18. C.W. Johnson, Phys. Rev. C **91**, 034313 (2015)
19. A.M. Shirokov, J.P. Vary, A.I. Mazur, T.A. Weber, Phys. Lett. B **644**, 33 (2007)
20. G.D. Gregorio, J. Herko, F. Knapp, N. Lo Iudice, P. Veselý, Phys. Rev. C **95**, 024306 (2017)
21. A.M. Shirokov, I.J. Shin, Y. Kim, M. Sosonkina, P. Maris, J.P. Vary, Phys. Lett. B **761**, 87 (2016). DOI 10.1016/j.physletb.2016.08.006
22. D.R. Entem, R. Machleidt, Phys. Rev. C **68**, 041001 (2003). DOI 10.1103/PhysRevC.68.041001
23. S.K. Bogner, R.J. Furnstahl, P. Maris, R.J. Perry, A. Schwenk, J. Vary, Nucl. Phys. A **801**, 21 (2008)
24. C. Forssen, J.P. Vary, E. Caurier, P. Navratil, Phys. Rev. C **77**, 024301 (2008)
25. P. Maris, J.P. Vary, A.M. Shirokov, Phys. Rev. C **79**, 014308 (2009)
26. S.A. Coon, M.I. Avetian, M.K.G. Kruse, U. van Kolck, P. Maris, J.P. Vary, Phys. Rev. C **86**, 054002 (2012)
27. R.J. Furnstahl, S.N. More, T. Papenbrock, Phys. Rev. C **89**, 044301 (2014)
28. R.J. Furnstahl, G. Hagen, T. Papenbrock, K.A. Wendt, J. Phys. G **42**, 034032 (2015)
29. M.A. Caprio, P.J. Fasano, J.P. Vary, P. Maris, J. Hartley, in *Proceedings of the International Conference Nuclear Theory in the Supercomputing Era 2018*, ed. by A.M. Shirokov, A.I. Mazur (Pacific National University, Khabarovsk, Russia, in press)
30. J. Chen, K. Auranen, M.L. Avila, B.B. Back, M.A. Caprio, C.R. Hoffman, D. Gorelov, B.P. Kay, S.A.

Kuvin, Q. Liu, J.L. Lou, A.O. Macchiavelli, D.G. McNeel, T.L. Tang, D. Santiago-Gonzalez, R. Talwar, J. Wu, G. Wilson, R.B. Wiringa, Y.L. Ye, C.X. Yuan, H.L. Zang, Phys. Rev. C (submitted)
31. M. Gell-Mann, Phys. Rev. **125**, 1067 (1962)
32. B.G. Wybourne, *Classical Groups for Physicists* (Wiley, New York, 1974)
33. A.O. Barut, R. Raczka, *Theory of Group Representations and Applications* (Polish Scientific Publishers, Warsaw, 1977)
34. F. Iachello, in *Group Theoretical Methods in Physics*, *Lecture Notes in Physics*, vol. 94, ed. by W. Beiglböck, A. Bohm, E. Takasugi (Springer-Verlag, Berlin, 1979), *Lecture Notes in Physics*, vol. 94, p. 420
35. J.P. Elliott, Proc. R. Soc. London A **245**, 128 (1958)
36. J.P. Elliott, Proc. R. Soc. London A **245**, 562 (1958)
37. J.P. Elliott, M. Harvey, Proc. R. Soc. London A **272**, 557 (1963)
38. J.P. Elliott, C.E. Wilsdon, Proc. R. Soc. London A **302**, 509 (1968)
39. G. Rosensteel, D.J. Rowe, Phys. Rev. Lett. **38**, 10 (1977)
40. D.J. Rowe, Rep. Prog. Phys. **48**, 1419 (1985)
41. D.J. Rowe, A.E. McCoy, M.A. Caprio, Physica Scripta **91**, 033003 (2016)
42. T. Dytrych, K.D. Sviratcheva, C. Bahri, J.P. Draayer, J.P. Vary, Phys. Rev. Lett. **98**, 162503 (2007)
43. T. Dytrych, K.D. Sviratcheva, C. Bahri, J.P. Draayer, J.P. Vary, Phys. Rev. C **76**, 014315 (2007)
44. J.P. Draayer, T. Dytrych, K.D. Launey, D. Langr, Prog. Part. Nucl. Phys. **67**, 516 (2012)
45. T. Dytrych, K.D. Launey, J.P. Draayer, P. Maris, J.P. Vary, E. Saule, U. Catalyurek, M. Sosonkina, D. Langr, M.A. Caprio, Phys. Rev. Lett. **111**, 252501 (2013). DOI 10.1103/PhysRevLett.111.252501
46. K.D. Launey, T. Dytrych, J.P. Draayer, Prog. Part. Nucl. Phys. **89**, 101 (2016)
47. A.E. McCoy, *Ab initio* multi-irrep symplectic no-core configuration interaction calculations. Ph.D. thesis, University of Notre Dame (2018). URL `https://curate.nd.edu/show/pz50gt57p16`
48. A.E. McCoy, M.A. Caprio, T. Dytrych, Phys. Rev. Lett. (submitted)
49. G. Alaga, K. Alder, A. Bohr, B.R. Mottelson, Mat. Fys. Medd. Dan. Vid. Selsk. **29**(9) (1955)
50. D.J. Rowe, *Nuclear Collective Motion: Models and Theory* (World Scientific, Singapore, 2010)
51. J. Suhonen, *From Nucleons to Nucleus* (Springer-Verlag, Berlin, 2007)
52. P. Maris, M. Sosonkina, J.P. Vary, E. Ng, C. Yang, Procedia Comput. Sci. **1**, 97 (2010). DOI 10.1016/j.procs.2010.04.012
53. H.M. Aktulga, C. Yang, E.G. Ng, P. Maris, J.P. Vary, Concurrency Computat.: Pract. Exper. **26**, 2631 (2013). DOI 10.1002/cpe.3129
54. M. Shao, H.M. Aktulga, C. Yang, E.G. Ng, P. Maris, J.P. Vary, Comput. Phys. Commun. **222**, 1 (2018)
55. D.R. Tilley, C.M. Cheves, J.L. Godwin, G.M. Hale, H.M. Hofmann, J.H. Kelley, C.G. Sheu, H.R. Weller, Nucl. Phys. A **708**, 3 (2002). DOI 10.1016/S0375-9474(02)00597-3
56. D.R. Tilley, J.H. Kelley, J.L. Godwin, D.J. Millener, J.E. Purcell, C.G. Sheu, H.R. Weller, Nucl. Phys. A **745**, 155 (2004)
57. J. Kelley, E. Kwan, J.E. Purcell, C.G. Sheu, H.R. Weller, Nucl. Phys. A **880**, 88 (2012)
58. W. von Oertzen, Z. Phys. A **357**, 355 (1997)
59. H.G. Bohlen, W. von Oertzen, R. Kalpakchieva, T.N. Massey, T. Dorsch, M. Milin, Ch. Schulz, Tz. Kokalova, C. Wheldon, J. Phys. Conf. Ser. **111**, 012021 (2008). DOI 10.1088/1742-6596/111/1/012021
60. A.E. McCoy, M.A. Caprio, T. Dytrych, Ann. Acad. Rom. Sci. Ser. Chem. Phys. Sci. **3**, 17 (2018). URL `http://www.aos.ro/wp-content/anale/PCVol3Nr1Art.2.pdf`
61. H. Hergert, Physica Scripta **92**, 023002 (2017)
62. D.R. Inglis, Rev. Mod. Phys. **25**, 390 (1953)
63. D. Kurath, Phys. Rev. **101**, 216 (1956)
64. R.R. Whitehead, in *Theory and Applications of Moment Methods in Many-Fermion Systems*, ed. by B.J. Dalton, S.M. Grimes, J.P. Vary, S.A. Williams (Plenum, New York, 1980), p. 235
65. G.J. Mathews, S.D. Bloom, K. Takahasi, G.M. Fuller, R.F. Hausman, Jr., in *International Symposium on Nuclear Shell Models*, ed. by M. Vallieres, B.H. Wildenthal (World Scientific, Philadelphia, 1985), p. 447
66. W.C. Haxton, K.M. Nollett, K.M. Zurek, Phys. Rev. C **72**, 065501 (2005)
67. V.G. Gueorguiev, J.P. Draayer, C.W. Johnson, Phys. Rev. C **63**, 014318 (2000)
68. D.J. Millener, Nucl. Phys. A **693**, 394 (2001)
69. J.S. Blair, E.M. Henley, Phys. Rev. **112**, 2029 (1958)
70. P.D. Kunz, Ann. Phys. (N.Y.) **11**, 275 (1960)
71. J. Hiura, I. Shimodaya, Prog. Theor. Phys. **30**, 585 (1963)

72. V. Della Rocca, F. Iachello, Nucl. Phys. A **973**, 1 (2018)
73. I. Talmi, I. Unna, Phys. Rev. Lett. **4**, 469 (1960)
74. C. Forssén, P. Navrátil, W.E. Ormand, E. Caurier, Phys. Rev. C **71**, 044312 (2005)
75. A. Calci, P. Navrátil, R. Roth, J. Dohet-Eraly, S. Quaglioni, G. Hupin, Phys. Rev. Lett. **117**, 242501 (2016)
76. Y. Kim, I.J. Shin, A.M. Shirokov, M. Sosonkina, P. Maris, J.P. Vary, in *Proceedings of the International Conference Nuclear Theory in the Supercomputing Era 2018*, ed. by A.M. Shirokov, A.I. Mazur (Pacific National University, Khabarovsk, Russia, in press)
77. Y. Kanada-En'yo, M. Kimura, A. Ono, Prog. Exp. Theor. Phys. **2012**, 01A202 (2012)
78. J.D. Rogers, Annu. Rev. Nucl. Sci. **15**, 241 (1965)
79. G. Rosensteel, D.J. Rowe, Ann. Phys. (N.Y.) **126**, 343 (1980)
80. A.E. McCoy, M.A. Caprio, T. Dytrych, in *Proceedings of the International Conference Nuclear Theory in the Supercomputing Era 2018*, ed. by A.M. Shirokov, A.I. Mazur (Pacific National University, Khabarovsk, Russia, in press)
81. R. Le Blanc, J. Carvalho, D.J. Rowe, Phys. Lett. B **140**, 155 (1984)
82. R. Le Blanc, J. Carvalho, M. Vassanji, D.J. Rowe, Nucl. Phys. A **452**, 263 (1986)
83. E.A. McCutchan, C.J. Lister, R.B. Wiringa, S.C. Pieper, D. Seweryniak, J.P. Greene, M.P. Carpenter, C.J. Chiara, R.V.F. Janssens, T.L. Khoo, T. Lauritsen, I. Stefanescu, S. Zhu, Phys. Rev. Lett. **103**, 192501 (2009)
84. E.A. McCutchan, C.J. Lister, S.C. Pieper, R.B. Wiringa, D. Seweryniak, J.P. Greene, P.F. Bertone, M.P. Carpenter, C.J. Chiara, G. Gürdal, C.R. Hoffman, R.V.F. Janssens, T.L. Khoo, T. Lauritsen, S. Zhu, Phys. Rev. C **86**, 014312 (2012). DOI 10.1103/PhysRevC.86.014312. URL `https://link.aps.org/doi/10.1103/PhysRevC.86.014312`
85. V.M. Datar, D.R. Chakrabarty, S. Kumar, V. Nanal, S. Pastore, R.B. Wiringa, S.P. Behera, A. Chatterjee, D. Jenkins, C.J. Lister, E.T. Mirgule, A. Mitra, R.G. Pillay, K. Ramachandran, O.J. Roberts, P.C. Rout, A. Shrivastava, P. Sugathan, Phys. Rev. Lett. **111**, 062502 (2013)
86. S.L. Henderson, T. Ahn, M.A. Caprio, P.J. Fasano, A. Simon, W. Tan, P. O'Malley, J. Allen, D.W. Bardayan, D. Blankstein, B. Frentz, M.R. Hall, J.J. Kolata, A.E. McCoy, S. Moylan, C.S. Reingold, S.Y. Strauss, R.O. Torres-Isea, Phys. Rev. C **99**, 064320 (2019). DOI 10.1103/PhysRevC.99.064320
87. Y. Suzuki, K.T. Hecht, Nucl. Phys. A **455**, 315 (1986)
88. K. Kravvaris, A. Volya, Phys. Rev. Lett. **119**, 062501 (2017)
89. M. Vorabbi, P. Navrátil, S. Quaglioni, G. Hupin, Phys. Rev. C **100**, 024304 (2019)